Algebraic approach to two-dimensional systems: Shape phase transitions, monodromy, and thermodynamic quantities

F. Pérez-Bernal*
Departamento de Física Aplicada, Facultad de Ciencias Experimentales, Universidad de Huelva, Campus del Carmen, Avenida de las Fuerzas Armadas, s/n 21071 Huelva, Spain

F. Iachello†
Center for Theoretical Physics, Sloane Physics Laboratory, Yale University, P.O. Box 208120, New Haven, Connecticut 06520-8120, USA
(Received 10 May 2007; revised manuscript received 1 December 2007; published 25 March 2008)

We analyze shape phase transitions in two-dimensional algebraic models. We apply our analysis to linear-to-bent transitions in molecules and point out what observables are particularly sensitive to the transition (order parameters). We study numerically the scaling behavior of observables and confirm the dependence of the energy gap for phase transitions of U(n)-SO($n+1$) type. We calculate energies of excited states and show their unusual behavior for some values of the Hamiltonian control parameter. This behavior is due to the double-humped nature of the potential and can be associated with the concept of monodromy. Finally, we compute numerically thermodynamic quantities, in particular heat capacities, and show their large variation at and around the critical value of the control parameter.

DOI: 10.1103/PhysRevA.77.032115 PACS number(s): 03.65.Fd, 05.70.Fh, 33.20.Vq, 05.70.Jk

I. INTRODUCTION

In recent years, algebraic models based on boson realizations of a Lie algebra U(n) have been shown to provide an effective description of many-body problems with $d=n-1$ degrees of freedom [1–3]. A vast variety of applications of such models has been worked out in nuclear and molecular physics, where algebraic models have been very successful in describing properties of rotational and vibrational spectra [4–6]. In these applications the number of bodies, N, is of order $N\sim 2-80$ in nuclear physics, where the bosons represent nucleon Cooper pairs [4], and $N\sim 2-300$ in molecular physics, where the bosons represent quanta of vibration (vibrons) [5]. A feature of these models is the occurrence of phases connected to specific configurations of the ground state, which arise, in algebraic models, from the occurrence of dynamic symmetries [1–3]. At the same time, algorithms have been developed to study ground-state phase transitions within the framework of algebraic models [7,8]. These phase transitions occur as a function of a control parameter ξ that appears in the Hamiltonian, conventionally written as $H(\xi)=(1-\xi)H_1+\xi H_2$, and are zero temperature phase transitions. The "phases" also correspond to geometric configurations of the ground state and thus the phase transitions are also called "shape phase transitions." In this paper, we investigate in detail phase transitions in $d=2$ algebraic models described by the Lie algebra U(3) [two-dimensional (2D) systems]. A generic study for interacting boson models in arbitrary dimension is given in [9]. Our study is applicable to linear-to-bent transitions in molecules, where the U(3) model was originally introduced [10] and also to models of high-T_c superconductors based on s-d wave pairing in 2D systems [11–13]. After a brief review of the algebraic structure of the model (Sec. II), we construct the ground-state energy functional by making use of boson coherent states, study its properties and show analytically that this system has a continuous phase transition in which discontinuity occurs in the second derivative of the ground-state energy and the first derivative of the order parameter for a critical value of the strength of the interaction between bosons [U(2)-SO(3) transition] (Sec. III). We also investigate numerically the behavior of observables (energies and electromagnetic transition rates) as a function of the number of bosons N (here the total number of vibrational quanta), both for the ground state and for the first few excited states and extract finite-size scaling exponents for several of them. Our study reveals an unusual behavior of the excited states in the region of the phase diagram with $\xi>\xi_c$, with the nature of the states abruptly changing at some value of the excitation energy. At this value we find also an accumulation of states which can be connected with the concept of quantum monodromy [14] (Sec. IV). Finally we calculate numerically the level densities, partition function, and heat capacity as a function of the control parameter and show that those too have an unusual behavior at $\xi\sim\xi_c$ (Sec. V). In particular, in the limit $N\to\infty$, the level density diverges at the critical value of the control parameter. Some features of the phase transitions discussed in this paper, especially those related to spectroscopic properties (energies and electromagnetic transition rates) can and actually have been experimentally observed, since there are some molecules which are at or close to the critical value of the control parameter [15,16]. The features associated with the accumulation of states at some energy (monodromy) have eluded for some time detection. However, recently it has become possible to detect them in the spectra of some molecules [17], primarily water [18]. The features of the heat capacity (a jump as a function of temperature) have not been detected. We have estimated the temperature at which the jump occurs in one molecule, HCNO, for which $\xi\simeq\xi_c$, and find that,

*francisco.perez@dfaie.uhu.es
†francesco.iachello@yale.edu; Also at Department of Chemistry, Yale University, P.O. Box 208107, New Haven, CT 06520-8107.

although difficult, it may be possible to detect the phase transitional behavior.

II. U(3) ALGEBRAIC APPROACH

In this section, we review the U(3) algebraic approach to 2D systems, introduced in [10] and present new formulas needed for a complete investigation of this system.

A. Bosonic U(3) algebra for 2D systems

The bosonic U(3) Lie algebra needed for 2D systems can be constructed with Cartesian boson creation and annihilation operators $\{\tau_x^\dagger, \tau_y^\dagger, \tau_x, \tau_y\}$ together with a scalar boson $\{\sigma^\dagger, \sigma\}$. The commutation relations between the creation and annihilation operators are

$$[\sigma, \sigma^\dagger] = 1, \quad [\tau_i, \tau_j^\dagger] = \delta_{i,j}, \quad [\tau_i, \sigma^\dagger] = 0; \ i,j = x,y. \quad (1)$$

All other commutators are zero. It is convenient to introduce circular bosons

$$\tau_\pm^\dagger = \mp \frac{\tau_x^\dagger \pm i\tau_y^\dagger}{\sqrt{2}}, \quad (2a)$$

$$\tau_\pm = \mp \frac{\tau_x \mp i\tau_y}{\sqrt{2}}. \quad (2b)$$

The annihilation operators in (2b) do not transform as spherical tensor operators [4–6]. We define operators that transform as spherical tensors

$$\tilde{\tau}_m = (-1)^{1-m}\tau_{-m}, \quad \tilde{\sigma} = \sigma, \quad (3)$$

and thus

$$\tilde{\tau}_\pm = \tau_\mp. \quad (4)$$

Circular bosons can be defined up to a phase. Our choice of phases (different from [10]) and the argument leading to Eq. (4) are discussed in Appendix A. The nine U(3) elements (generators) of U(3) are the bilinear products of creation and annihilation operators. They can be written as [10]

$$\hat{n} = \tau_+^\dagger\tau_+ + \tau_-^\dagger\tau_-, \quad \hat{n}_s = \sigma^\dagger\sigma,$$

$$\hat{l} = \tau_+^\dagger\tau_+ - \tau_-^\dagger\tau_-,$$

$$\hat{D}_+ = \sqrt{2}(\tau_+^\dagger\sigma - \sigma^\dagger\tau_-), \quad \hat{D}_- = \sqrt{2}(-\tau_-^\dagger\sigma + \sigma^\dagger\tau_+),$$

$$\hat{Q}_+ = \sqrt{2}\tau_+^\dagger\tau_-, \quad \hat{Q}_- = \sqrt{2}\tau_-^\dagger\tau_+,$$

$$\hat{R}_+ = \sqrt{2}(\tau_+^\dagger\sigma + \sigma^\dagger\tau_-), \quad \hat{R}_- = \sqrt{2}(\tau_-^\dagger\sigma + \sigma^\dagger\tau_+). \quad (5)$$

The operators in (5) have physical meaning. The operator $\hat{l}$, for example, is the angular momentum in 2D, as one can easily see by returning to Cartesian boson operators

$$\tau_+^\dagger\tau_+ - \tau_-^\dagger\tau_- = -i(\tau_x^\dagger\tau_y - \tau_y^\dagger\tau_x), \quad (6)$$

and from these to coordinates

$$\hat{l} = -i\left(x\frac{\partial}{\partial y} - y\frac{\partial}{\partial x}\right). \quad (7)$$

We next consider the possible subalgebra chains. There are two possible chains starting from U(3) and ending in SO(2) (i.e., that conserve 2D angular momentum),

$$\mathrm{U}(3) \supset \mathrm{U}(2) \supset \mathrm{SO}(2), \quad \text{Chain (I)}, \quad (8a)$$

$$\mathrm{U}(3) \supset \mathrm{SO}(3) \supset \mathrm{SO}(2), \quad \text{Chain (II)}. \quad (8b)$$

The corresponding subalgebras are composed by the following elements:

$$\mathrm{U}(2) \quad \{\hat{n}, \hat{l}, \hat{Q}_+, \hat{Q}_-\},$$

$$\mathrm{SO}(3) \quad \{\hat{l}, \hat{D}_+, \hat{D}_-\},$$

$$\mathrm{SO}(2) \quad \{\hat{l}\}, \quad (9)$$

where the SO(3) elements satisfy the usual angular momentum commutation relations. Because of an automorphism of the Lie algebra U(3) constructed with $\tau_\pm$, σ there is an alternative SO(3) subalgebra of U(3), called $\overline{\mathrm{SO}(3)}$, with elements

$$\overline{\mathrm{SO}(3)} \quad \{\hat{l}, \hat{R}_+, \hat{R}_-\}. \quad (10)$$

Another ingredient of the algebraic approach is the Casimir (or invariant) operators associated to each subalgebra chain [1–3]. The first- and second-order Casimir operators for the subalgebras in Eqs. (9) and (10) are

$$\hat{C}_1[\mathrm{U}(2)] = \hat{n}, \quad \hat{C}_2[\mathrm{U}(2)] = \hat{n}(\hat{n}+1),$$

$$\hat{C}_2[\mathrm{SO}(3)] = \hat{W}^2 = (\hat{D}_+\hat{D}_- + \hat{D}_-\hat{D}_+)/2 + \hat{l}^2,$$

$$\hat{C}_1[\mathrm{SO}(2)] = \hat{l}, \quad \hat{C}_2[\mathrm{SO}(2)] = \hat{l}^2, \quad (11)$$

and

$$\hat{C}_2[\overline{\mathrm{SO}(3)}] = (\hat{R}_+\hat{R}_- + \hat{R}_-\hat{R}_+)/2 + \hat{l}^2. \quad (12)$$

The most general rotation, parity-invariant, one- and two-body Hamiltonian can be written as a linear combination of first- and second-order invariants of chains (8a) and (8b).

$$\hat{H} = E_0 + \epsilon\hat{C}_1[\mathrm{U}(2)] + \alpha\hat{C}_2[\mathrm{U}(2)] + \beta\hat{C}_2[\mathrm{SO}(2)] + A\hat{C}_2[\mathrm{SO}(3)]. \quad (13)$$

This Hamiltonian can be rewritten in various forms. For example, the SO(3) Casimir operator $\hat{W}^2$ can be replaced by the pairing operator

$$\hat{P} = N(N+1) - \hat{W}^2. \quad (14)$$

Here, the total number operator, $\hat{N} = \hat{n}_s + \hat{n}$, has been replaced by its value N, due to the fact that we consider systems with a fixed number of bosons, N. The Hamiltonian can then be rewritten as

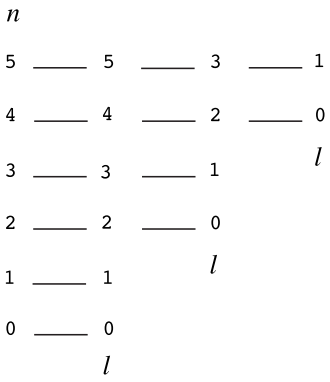

FIG. 1. Energy spectrum of the cylindrical oscillator associated to chain (I), Eq. (19), with parameters $\beta=0$, $\alpha=0$, and $\epsilon=1.0$. Levels up to $n=5$ are shown. Levels with $l\neq 0$ are doubly degenerate, $\pm l$.

$$\hat{H} = E_0' + \epsilon\hat{n} + \alpha\hat{n}(\hat{n}+1) + \beta\hat{l}^2 + A'\hat{P}, \tag{15}$$

where $E_0'=E_0+N(N+1)$ and $A'=-A$.

B. Dynamical symmetries

The two chains of subalgebras of Eqs. (8a) and (8b) imply the existence of two dynamical symmetries of the Hamiltonian, that is, situations in which the Hamiltonian can be written in terms only of Casimir operators of a chain.

1. Chain (I): Cylindrical oscillator chain

We call chain (I) the cylindrical oscillator chain. We denote states by the quantum numbers

$$\left|\begin{matrix} \mathrm{U}(3) & \supset & \mathrm{U}(2) & \supset & \mathrm{SO}(2) \\ [N] & & n & & l \end{matrix}\right\rangle, \tag{16}$$

and label them by $|[N];n,l\rangle$. An alternative notation, often used in molecular physics, is $|[N];n^l\rangle$. The quantum number N labels the totally symmetric representation of U(3), $[N]$, and it is related to the total number of bound states of the system, n is the vibrational quantum number, and l is the 2D angular momentum. The branching rules are

$$n = N, N-1, N-2, \ldots, 0,$$

$$l = \pm n, \pm(n-2), \ldots, \pm 1 \text{ or } 0 \quad (n = \text{odd or even}). \tag{17}$$

The Hamiltonian is

$$\hat{H}^{(\mathrm{I})} = E_0 + \epsilon\hat{C}_1[\mathrm{U}(2)] + \alpha\hat{C}_2[\mathrm{U}(2)] + \beta\hat{C}_2[\mathrm{SO}(2)] \tag{18}$$

with eigenvalues

$$E^{(\mathrm{I})}(n,l) = E_0 + \epsilon n + \alpha n(n+1) + \beta l^2. \tag{19}$$

The eigenvalues of (18), schematically depicted in Fig. 1, are those of a truncated anharmonic two-dimensional oscillator, since $n\leq N$. The present chain, when applied to molecular vibrations, describes bending vibrations of rigidly linear molecules.

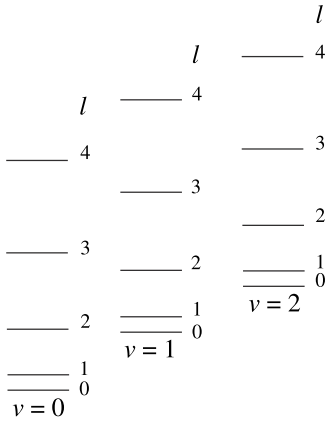

FIG. 2. Energy spectrum of the two-dimensional displaced oscillator associated to chain (II), Eq. (25), with parameters $N=10$, $\beta=0.5$, and $A=-0.1$. The first three vibrational bands, $v=0,1,2$, with $l\leq 4$ are shown. Levels with $l\neq 0$ are doubly degenerate, $\pm l$.

2. Chain (II): Displaced oscillator chain

We call chain (II) the displaced oscillator chain. States are characterized by the quantum numbers

$$\left|\begin{matrix} \mathrm{U}(3) & \supset & \mathrm{SO}(3) & \supset & \mathrm{SO}(2) \\ [N] & & \omega & & l \end{matrix}\right\rangle. \tag{20}$$

States in this chain will be labelled as $|[N];\omega,l\rangle$. The branching rules are

$$\omega = N, N-2, N-4, \ldots, 1 \text{ or } 0 \quad (N = \text{odd or even}),$$

$$l = \pm\omega, \pm(\omega-1), \ldots, 0. \tag{21}$$

In this case, it is convenient to introduce a vibrational quantum number v, which can be identified with the number of quanta of excitation in the displaced oscillator,

$$v = \frac{N-\omega}{2}. \tag{22}$$

The branching rules are

$$v = 0, 1, \ldots, \frac{N-1}{2} \text{ or } \frac{N}{2} \quad (N = \text{odd or even}),$$

$$l = 0, \pm 1, \pm 2, \ldots, \pm(N-2v). \tag{23}$$

The Hamiltonian is

$$\hat{H}^{(\mathrm{II})} = E_0 + \beta\hat{C}_2[\mathrm{SO}(2)] + A\hat{C}_2[\mathrm{SO}(3)] \tag{24}$$

with eigenvalues

$$E^{(\mathrm{II})}(\omega,l) = E_0 + \beta l^2 + A\omega(\omega+1)$$
$$= E_0' + \beta l^2 - 4A[(N+1/2)v - v^2]. \tag{25}$$

The corresponding spectrum is that of a displaced anharmonic two-dimensional oscillator and is depicted in Fig. 2.

C. Transformation brackets

In the cylindrical oscillator chain (I) the expression of the basis states in terms of boson creation and annihilation operators is rather simple

$$|[N];n,l\rangle = \mathcal{N}_{nl}^{N}(\sigma^{\dagger})^{N-n}(\tau_{+}^{\dagger})^{(n+l)/2}(\tau_{-}^{\dagger})^{(n-l)/2}|0\rangle, \tag{26}$$

with normalization constant

$$\mathcal{N}_{nl}^{N} = \frac{1}{\sqrt{(N-n)!\left(\frac{n+l}{2}\right)!\left(\frac{n-l}{2}\right)!}}. \tag{27}$$

For purposes of calculating matrix elements it is convenient to expand the eigenstates of the displaced oscillator chain (II) into (I). This is achieved by means of the transformation brackets

$$\langle [N];n,l|[N];\omega,l\rangle = (-1)^{N-\omega-l+\mathrm{mod}(l,2)/2}2^{n/2-\omega}\sqrt{\frac{(2\omega+1)(\omega-l)!\left(\frac{n+l}{2}\right)!(N-n)!}{(N-\omega)!\,!\,(N+\omega+1)!\,!\left(\frac{n-l}{2}\right)!(\omega+l)!}}$$
$$\times \sum_{\substack{m=0 \\ n-l\leq N-\omega+2m}}^{(\omega-l/2)} \frac{(-1)^m(2\omega-2m)!\left(\frac{N-\omega+2m}{2}\right)!}{(\omega-m)!\,m!\,(\omega-2m-l)!\left(\frac{N-\omega-n+l+2m}{2}\right)!}. \tag{28}$$

A detailed derivation of this formula can be found in Appendix B.

D. Operator matrix elements

In this section we present analytical expressions for the matrix elements of the generators of the U(3) algebra in the two bases associated to the possible dynamical symmetries of Eqs. (8a) and (8b). Although numerical calculations are usually done in the cylindrical oscillator basis (I), given in Eq. (16), we give for completeness the matrix elements in the displaced oscillator basis (II).

1. Cylindrical oscillator basis

The matrix elements of the boson operators $\sigma^{\dagger}$ and $\tau_{\pm}^{\dagger}$ can be easily evaluated in the basis states of Eq. (26),

$$\langle [N+1];n,l|\sigma^{\dagger}|[N];n,l\rangle = \sqrt{N-n+1}, \tag{29a}$$

$$\langle [N+1];n+1^{l\pm1}|\tau_{\pm}^{\dagger}|[N];n,l\rangle = \sqrt{\frac{n\pm l+2}{2}}. \tag{29b}$$

From these, one can obtain the matrix elements of any combination of boson creation and annihilation operators. The matrix elements of the generators of the algebra are

$$\langle [N];n,l|\hat{n}_s|[N];n,l\rangle = N-n, \tag{30a}$$

$$\langle [N];n,l|\hat{n}|[N];n,l\rangle = n, \tag{30b}$$

$$\langle [N];n,l|\hat{l}|[N];n,l\rangle = l, \tag{30c}$$

$$\langle [N];n+1,l\pm1|\hat{D}_{\pm}|[N];n,l\rangle = \pm\sqrt{(N-n)(n\pm l+2)}, \tag{30d}$$

$$\langle [N];n+1,l\pm1|\hat{R}_{\pm}|[N];n,l\rangle = \sqrt{(N-n)(n\pm l+2)}, \tag{30e}$$

$$\langle [N];n,l\pm2|\hat{Q}_{\pm}|[N];n,l\rangle = \sqrt{(n\mp l)(n\pm l+2)}. \tag{30f}$$

2. Displaced oscillator chain

The formulas derived in Appendix B, especially the expression of the displaced oscillator basis states in terms of boson creation operators, allow one to calculate matrix elements of the boson operators in the basis (II).

For example, the matrix elements of $\sigma^{\dagger}$ are given by

$$\langle [N+1];\omega_2,l|\sigma^{\dagger}|[N];\omega_1,l\rangle = \left(\frac{(N+\omega_1+3)(\omega_1-l+1)(\omega_1+l+1)}{(2\omega_1+1)(2\omega_1+3)}\right)^{1/2}\delta_{\omega_2,\omega_1+1} - \left(\frac{(N-\omega_1+2)(\omega_1-l)(\omega_1+l)}{(2\omega_1+1)(2\omega_1-1)}\right)^{1/2}\delta_{\omega_2,\omega_1-1}. \tag{31}$$

The matrix elements for the annihilation operator σ can be computed taking the Hermitian conjugates of the previous equation. The matrix elements of the $\hat{n}_s=\sigma^{\dagger}\sigma$ operator can then be deduced

$$\langle [N];\omega_2,l|\hat{n}_s|[N];\omega_1,l\rangle = A_0(N,\omega_1,l)\,\delta_{\omega_2,\omega_1} - B_0(N,\omega_1,l)\,\delta_{\omega_2+2,\omega_1} - B_1(N,\omega_1,l)\,\delta_{\omega_2-2,\omega_1}, \tag{32}$$

where we have made use of the fact that both N and l are good quantum numbers in the SO(3) chain. The factors $A_0(N,\omega,l)$, $B_0(N,\omega,l)$, and $B_1(N,\omega,l)$ are

$$A_0(N,\omega,l) = \frac{(N-\omega)(\omega+l+1)(\omega-l+1)}{(2\omega+1)(2\omega+3)} + \frac{(N+\omega+1)(\omega+l)(\omega-l)}{(2\omega-1)(2\omega+1)}, \tag{33a}$$

$$B_0(N,\omega,l) = \left(\frac{(N-\omega)(N+\omega+3)(\omega-l+2)(\omega+l+2)(\omega+l+1)(\omega-l+1)}{(2\omega+1)(2\omega+3)^2(2\omega+5)}\right)^{1/2}, \tag{33b}$$

$$B_1(N,\omega,l) = \left(\frac{(N-\omega+2)(N+\omega+1)(\omega-l)(\omega+l)(\omega+l-1)(\omega-l-1)}{(2\omega-3)(2\omega-1)^2(2\omega+1)}\right)^{1/2}. \tag{33c}$$

Similarly, the matrix elements of $\tau_\pm^\dagger$ are found to be

$$\langle [N+1];\omega_2,l\pm 1|\tau_\pm^\dagger|[N];\omega_1,l_1\rangle = \left(\frac{(N+\omega_1+3)(\omega_1\pm l+1)(\omega_1\pm l+2)}{2(2\omega_1+1)(2\omega_1+3)}\right)^{1/2}\delta_{\omega_2,\omega_1+1} + \left(\frac{(N-\omega_1+2)(\omega_1\mp l)(\omega_1\mp l-1)}{2(2\omega_1+1)(2\omega_1-1)}\right)^{1/2}\delta_{\omega_2,\omega_1-1}. \tag{34}$$

Taking the Hermitian conjugate of the previous equation one can obtain the matrix elements of the annihilation operators $\tau_\pm$, and hence the matrix elements of $\hat{n}_\pm = \tau_\pm^\dagger\tau_\pm$,

$$\langle [N];\omega_2,l|\hat{n}_\pm|[N];\omega_1,l\rangle = \left(\frac{(N-\omega_1)(\omega_1\mp l+1)(\omega_1\mp l+1)}{(2\omega_1+1)(2\omega_1+3)} + \frac{(N+\omega_1+1)(\omega_1\pm l)(\omega_1\pm l-1)}{(2\omega_1-1)(2\omega_1+1)}\right)\delta_{\omega_2,\omega_1} + B_0(N,\omega_1,l)\,\delta_{\omega_2+2,\omega_1} - B_1(N,\omega_1,l)\,\delta_{\omega_2-2,\omega_1}, \tag{35}$$

where, as in the $\hat{n}_s$ case, we have made use of the fact that both N and l are good quantum numbers in the SO(3) chain. The factors $B_0(N,\omega,l)$ and $B_1(N,\omega,l)$ are defined in Eq. (33a)–(33c). The matrix elements of $\hat{n}_s$, Eq. (30a)–(30f), and the matrix elements of $\hat{n}=\hat{n}_+ + \hat{n}_-$ are trivially related by the relation $\hat{n}=\hat{N}-\hat{n}_s$.

Once the matrix elements of the scalar, $\sigma^\dagger$, and circular, $\tau_\pm^\dagger$, bosons are known, one can compute the matrix elements of the generators. The matrix elements of $\hat{D}_\pm$ are

$$\langle [N];\omega_2,l\pm 1|\hat{D}_\pm|[N];\omega_1,l\rangle = \sqrt{(\omega_1\pm l+1)(\omega_1\mp l)}\,\delta_{\omega_2,\omega_1}. \tag{36}$$

The expression for the generators $\hat{R}_\pm$ is slightly more involved. The matrix elements of $\hat{R}_-$ are

$$\langle [N];\omega_2,l_2|\hat{R}_-|[N];\omega_1,l_1\rangle = \frac{(2N+3)(2l_1-1)}{(2\omega_1-1)(2\omega_1+3)}\sqrt{\frac{(\omega_1-l_1+1)(\omega_1+l_1)}{2}}\,\delta_{\omega_2,\omega_1}\delta_{l_2,l_1-1} - \sqrt{\frac{C_0(N,\omega_1,l_1)}{(2\omega_1+1)(2\omega_1-1)^2(2\omega_1-3)}}\,\delta_{\omega_2,\omega_1-2}\delta_{l_2,l_1-1} + \sqrt{\frac{C_1(N,\omega_1,l_1)}{(2\omega_1+1)(2\omega_1+3)^2(2\omega_1+5)}}\,\delta_{\omega_2,\omega_1+2}\delta_{l_2,l_1-1}, \tag{37}$$

with

$$C_0(N,\omega,l) = 2(N+\omega+1)(N-\omega+2)(\omega+l)(\omega-l)(\omega+l-1)(\omega+l-2), \tag{38a}$$

$$C_1(N,\omega,l) = 2(N+\omega+3)(N-\omega)(\omega+l+1)(\omega-l+1)(\omega-l+2)(\omega-l+3). \tag{38b}$$

The matrix elements of $\hat{R}_+$ can be obtained from the Hermitian conjugate of the previous expression.

E. Two-body Hamiltonian

The most general, l conserving, two-body Hamiltonian can be expressed in terms of the operators $\hat{n}$, $\hat{n}^2$, $\hat{l}^2$, and $\hat{P}$. We will make use of the fact that N and l are good quantum numbers as their associated algebras belong to both dynamical symmetries. Using the expressions found in the preceding section we now calculate the Hamiltonian matrix elements in the cylindrical oscillator basis. The operators $\hat{n}$, $\hat{n}(\hat{n}+1)$, and $\hat{l}^2$ belong to this chain (8a), and thus they are diagonal

$$\langle [N];n_2,l|\hat{n}|[N];n_1,l\rangle = n_1\delta_{n_2,n_1},$$

$$\langle [N];n_2,l|\hat{n}(\hat{n}+1)|[N];n_1,l\rangle = n_1(n_1+1)\delta_{n_2,n_1},$$

$$\langle [N];n_2,l|\hat{l}^2|[N];n_1,l\rangle = l^2\delta_{n_2,n_1}. \tag{39}$$

The only nondiagonal operator is the SO(3) Casimir operator, $\hat{W}^2$, of Eq. (11). Its matrix elements can be derived from Eqs. (30a)–(30f),

$$\langle [N];n_2,l|\hat{W}^2|[N];n_1,l\rangle = [(N-n_1)(n_1+2)+(N-n_1+1)n_1+l^2]\delta_{n_2,n_1} - \sqrt{(N-n_1+2)(N-n_1+1)(n_1+l)(n_1-l)}\,\delta_{n_2,n_1-2} - \sqrt{(N-n_1)(N-n_1-1)(n_1+l+2)(n_1-l+2)}\,\delta_{n_2,n_1+2}. \tag{40}$$

As we have already noted, the pairing operator (14) is often used instead of $\hat{W}^2$. Its matrix elements can be trivially obtained from Eq. (40) because the $N(N+1)$ contribution is diagonal.

Any other two-body operator can be rewritten in terms of the previous four. For example, operators of interest are the quadratic Casimir operator of the $\overline{\mathrm{SO}(3)}$ algebra generated by $\{\hat{R}_\pm,\hat{l}\}$ and the quadrupole interaction $\hat{Q}\cdot\hat{Q}$. In the former case, the calculation is straightforward. The matrix elements are as in (40), but with nondiagonal matrix elements of opposite sign. The quadrupole interaction is constructed by coupling the $\hat{Q}_\pm$ operators defined in Eq. (5) as

$$\hat{Q}\cdot\hat{Q} = \hat{Q}_+\hat{Q}_- + \hat{Q}_-\hat{Q}_+ = 2(\hat{n}+2\tau_+^\dagger\tau_-^\dagger\tau_+\tau_-). \tag{41}$$

This interaction can be rewritten in terms of the Casimir operators of algebras of chain (I) and thus it is diagonal in the basis of Eq. (16),

$$\langle [N];n_2,l|\hat{Q}\cdot\hat{Q}|[N];n_1,l\rangle = (2n_1+n_1^2-l^2)\delta_{n_2,n_1}. \tag{42}$$

Therefore, both the quadratic Casimir operator of the $\overline{\mathrm{SO}(3)}$ algebra and $\hat{Q}\cdot\hat{Q}$ can be built as a combination of the two-body interactions discussed previously.

III. SHAPE PHASE TRANSITIONS IN THE U(3) APPROACH

Phase transitions in algebraic models can be studied by considering the general Hamiltonian (13) written in terms of Casimir operators of all chains [7,8,19]. However, since the algebra SO(2) is a common subalgebra to both chains, it is not relevant to the study of phase transitions. Furthermore, the quadratic Casimir operator of U(2), $\hat{C}_2[\mathrm{U}(2)]$, can be written as $\hat{C}_1[\mathrm{U}(2)]^2+\hat{C}_1[\mathrm{U}(2)]$ and its eigenfunctions are the same as those of $\hat{C}_1[\mathrm{U}(2)]$. Phase transitions in the U(3) approach can therefore be studied by considering the "essential" Hamiltonian

$$\hat{H} = \epsilon\hat{C}_1[\mathrm{U}(2)] + A\hat{C}_2[\mathrm{SO}(3)]. \tag{43}$$

It is convenient to rewrite this Hamiltonian, up to a constant term, in the form

$$\hat{\mathcal{H}} = \epsilon\left((1-\xi)\hat{n} + \frac{\xi}{N-1}\hat{P}\right). \tag{44}$$

Here we have made use of Eqs. (11) and (14), put the overall energy scale ϵ in front, and introduced the dimensionless control parameter $\xi\in[0,1]$. At $\xi=0$ the system is in phase (I), i.e., the eigenvalues and eigenstates of $\hat{\mathcal{H}}$ are those of the dynamic symmetry (I), while at $\xi=1$ the system is in phase (II), i.e., the eigenvalues and eigenstates are those of symmetry (II). The factor $1/(N-1)$ is introduced to take into account the fact that $\hat{P}$ is a two-body operator, while $\hat{n}$ is a one-body operator. One-body operators scale as N while two-body operators scale as $N(N-1)$.

A. Quantal aspects

The quantal aspects of the phase transition can be studied by diagonalizing the Hamiltonian $\hat{\mathcal{H}}$ as a function of the control parameter, ξ. The Hamiltonian $\hat{\mathcal{H}}$ is block diagonal and the 2D angular momentum l is a good quantum number. The dimension of a block with 2D angular momentum l for the totally symmetric representation $[N]$ of U(3) is $(N-|l|)/2+1$, if N and l have the same parity, and $(N-|l|+1)/2$ if they have different parity.

We now analyze the behavior of energies and intensities for this simple Hamiltonian as the control parameter ξ varies from zero to one, thus moving from chain (I) to chain (II).

1. Dependence on ξ of the energies

Preliminary studies of the spectrum associated to the model Hamiltonian (44) were presented in Refs. [10,15]. The behavior of energies as a function of ξ is shown in Fig. 3 for $N=8$. For the two limiting cases, $\xi=0$ and $\xi=1$, the energies are given by analytic formulas, Eq. (19) and Eq. (25), while for other values of ξ they are obtained numerically. This diagram is also known as the correlation energy diagram, and was originally presented in the framework of potential models [20,21].

The energy correlation diagram reveals the drastic changes that affect the spectrum when moving from $\xi=0$ to $\xi=1$. Four possible situations can be distinguished.

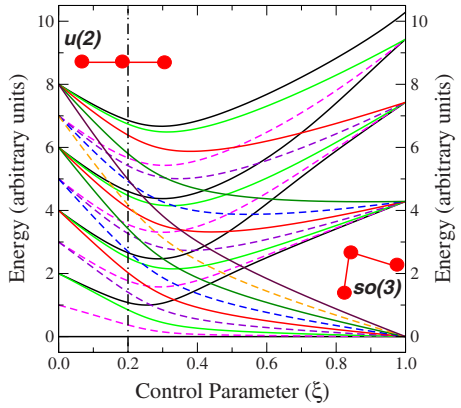

FIG. 3. (Color online) Correlation energy diagram obtained after diagonalization of the Hamiltonian in Eq. (44) for $N=8$ and energy scale $\epsilon=1$. Ground-state energies have been fixed to zero and the critical value of the control parameter $\xi_c=0.2$ has been marked with a vertical dotted-dashed line. Full (dashed) lines correspond to even (odd) vibrational angular momentum states.

(1) Rigidly linear case, $\xi=0$. The spectrum corresponds to a two-dimensional truncated harmonic oscillator with the corresponding l degeneracy and levels that can be unambiguously labelled by $|n,l\rangle$ [dynamic symmetry (I), Fig. 1]. The n and l values associated with degenerate levels have the same parity.

(2) Quasilinear case, $0<\xi\leq 0.2$. In this case the main feature is the appearance of positive anharmonicity. The degeneracy in l is broken, with smaller energy values for increasing values of l.

(3) Quasibent case, $0.2<\xi<1$. This situation is characterized by the appearance of a sign changing anharmonicity: Negative for the low-lying states becoming positive at high energy. The l degeneracy is also broken. In molecular physics this situation displaying first negative and then positive anharmonicities is known as the Dixon dip [22].

(4) Rigidly bent case, $\xi=1$. The spectrum is that of a two-dimensional truncated rovibrator [dynamic symmetry (II), Fig. 2]. The l quantum number corresponds to the angular momentum projection on the figure axis, usually labelled K, and the corresponding rotational bands on top of a vibrational head can be seen. The appropriate basis for this limit is formed by the states $|v,l\rangle$ associated to chain (II), where v, defined in Eq. (22), corresponds to the number of quanta of vibrational excitation.

In order to elucidate the previous statements and to explore the N dependence of the energy spectrum (scaling behavior), we show in Fig. 4 the energy as a function of a normalized vibrational quantum number $\nu=2u/N$ for different values of ξ. Here u labels the vibrational states, $u=0,1,2,\ldots,(N-1)/2$ or $N/2$ (N odd or even). In the limit $N\rightarrow\infty$ the label ν becomes a continuous variable defined in the interval [0,1]. To the right of $\xi=0.2$, $u\equiv v$, while to the left $u\equiv n/2$. The four selected ξ values are representative of the previously described situations and, in each case, results for three different values of N have been plotted, $N=40$, 100, and 400. The energy spectra in the four panels are qualitatively different, but these differences are particularly clear in

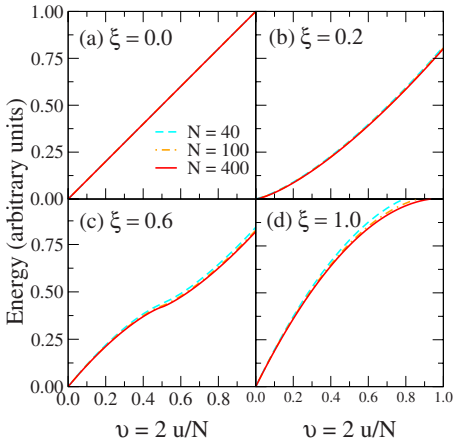

FIG. 4. (Color online) The four panels depict the energy of the $l=0$ vibrational excitations as a function of $\nu=2u/N$ for $N=40,100,400$. The values of the control parameter are $\xi=0.0$, 0.2, 0.6, and 1.0 for panels (a), (b), (c), and (d), respectively. The energy units are arbitrary and the energy scale is fixed to $\epsilon=1$. Ground-state energies have been set to zero.

an anharmonicity plot, called Birge-Sponer plot, of the energy differences $E_{\nu+1}-E_\nu$ as a function of ν. The anharmonicity plot that corresponds to the spectra in Fig. 4 is shown in the four panels of Fig. 5.

We have also studied the behavior of the energy levels with a normalized vibrational angular momentum $\lambda=l/N$, shown in Fig. 6. We observe here a change from linear behavior at $\xi=0$ to a quadratic behavior at $\xi=0.6$. For $\xi=1$ the energy is constant at zero due to the fact that we have used a simplified Hamiltonian, Eq. (44), for our study. Addition of $\hat{C}_2[\mathrm{SO}(2)]$ with coefficient β as in (13), will introduce a contribution βl^2 to the energies which will lift the degeneracy of the rotational states at $\xi=1$.

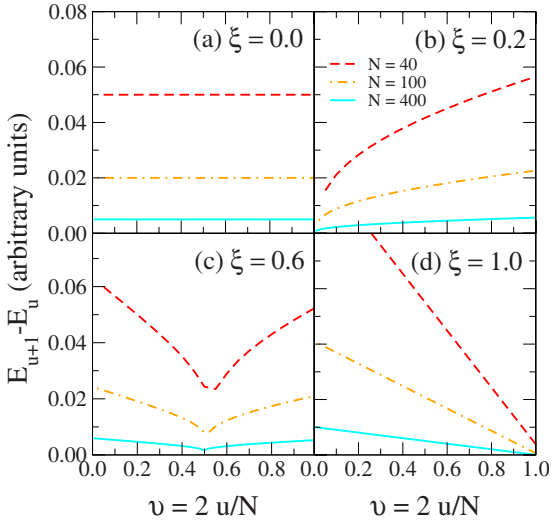

FIG. 5. (Color online) Birge-Sponer or anharmonicity plot where the energy difference $E_{u+1}-E_u$ is plotted as a function of $\nu=2u/N$ for $N=40,100,400$. The values of the control parameter are $\xi=0.0$, 0.2, 0.6, and 1.0 for panels (a), (b), (c), and (d), respectively. Energy units are arbitrary and the energy scale $\epsilon=1$.

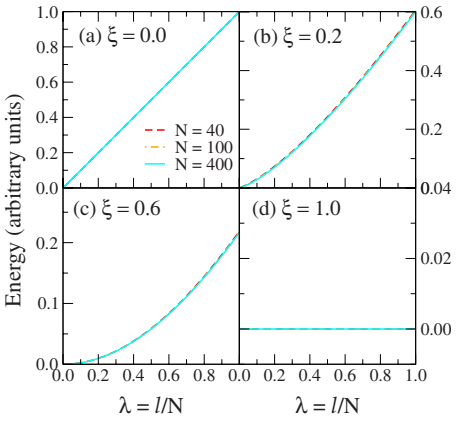

FIG. 6. (Color online) Rotational excitation plot, where the $v=0$ rotational band energies are plotted as a function of $\lambda=l/N$ for $N=40,100,400$. The values of the control parameter are $\xi=0.0$, 0.2, 0.6, and 1.0 for panels (a), (b), (c), and (d), respectively. Energy units are arbitrary and the energy scale $\epsilon=1$. Ground-state energy has been set to zero.

2. Dependence on ξ of the intensities

The variation of the control parameter not only affects the energy spectrum but also the nature of the resulting eigenfunctions. The wave-function dependence on ξ gives way to dramatic changes in the line intensities when moving between the two possible dynamical symmetries. In order to quantify these effects one needs to define the relevant transition operators, diagonalize the Hamiltonian as a function of the control parameter ξ, and compute matrix elements of the transition operators. A preliminary application of this procedure to the study of infrared intensity amplitudes of the carbon trimer (C_3) was presented in [16]. Following [10], we define the infrared transition operator as

$$\hat{T}^{\mathrm{IR}}_{\pm}=\frac{t}{\sqrt{N}}\hat{D}_{\pm}. \tag{45}$$

The matrix elements of this operator in the U(2) basis are

$$\langle[N];n+1;l\pm 1|\hat{T}^{\mathrm{IR}}_{\pm}|[N];n,l\rangle=\pm t\sqrt{(n\pm l+2)(1-n/N)}, \tag{46}$$

while in the SO(3) basis are

$$\langle[N];\omega_2,l\pm 1|\hat{T}^{\mathrm{IR}}_{\pm}|[N];\omega_1,l\rangle = \frac{t}{\sqrt{N}}\sqrt{(\omega_1\pm l+1)(\omega_1\mp l)}\,\delta_{\omega_2,\omega_1}. \tag{47}$$

The operators $\hat{T}^{\mathrm{IR}}_{\pm}$ add and subtract one unit of angular momentum. The intensities

$$I_{2\to 1}\propto|\langle\psi_2|\hat{T}^{\mathrm{IR}}_{+}|\psi_1\rangle|^2+|\langle\psi_2|\hat{T}^{\mathrm{IR}}_{-}|\psi_1\rangle|^2 \tag{48}$$

are shown as a function of ξ in Fig. 7 for transitions that are allowed [panel (a), $\Delta n=1$] and forbidden [panel (b), $\Delta n=3,5$] in the U(2) limit. Both show a jump around $\xi=0.2$.

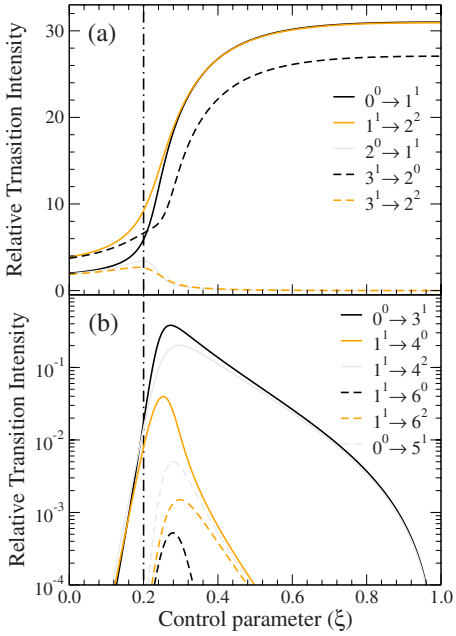

FIG. 7. (Color online) Infrared transition intensity for selected allowed-panel (a) and forbidden-panel (b) excitations as a function of the control parameter ξ of the model Hamiltonian (44). Panel (b) includes $\Delta n=3$ (full lines) and $\Delta n=5$ (dashed lines) forbidden transitions. All calculations were carried out with $N=40$. The molecular physics notation n^l is used to label the states.

B. Classical aspects

The quantal study of energies and intensities presented in the preceding section shows phase transitional behavior appearing at or around $\xi=0.2$. In order to understand whether or not the rapid variations seen numerically in some quantities are indeed related to phase transitions, it is convenient to make use of an algorithm introduced by Gilmore [7,8,19], which allows one to take the limit $N\to\infty$ (called classical or mean-field limit). The limit is called classical because the algorithm produces a classical Hamiltonian in terms of coordinates and momenta, $\alpha_i\equiv(q_i,p_i)$, here in two dimensions, x, y, p_x, and p_y, upon which a Landau analysis of the phase transition can be done, and mean field because it was shown long ago by Gilmore and Feng [19] that by minimizing the ground-state expectation value of the "intensive" Hamiltonian H (i.e., one that is regular as $N\to\infty$), one obtains an approximation to the ground-state energy E_0/N which converges to the exact energy when $N\to\infty$. In making use of the algorithm, we begin by introducing the coherent (or intrinsic) ground state

$$|[N];r,\theta\rangle=\frac{1}{\sqrt{N!}}(b_c^{\dagger})^N|0\rangle, \tag{49}$$

where r and θ are the polar coordinates associated to x and y and $b_c^{\dagger}$ is the boson condensate

$$b_c^{\dagger}=\frac{1}{\sqrt{1+r^2}}[\sigma^{\dagger}+(x\tau_x^{\dagger}+y\tau_y^{\dagger})]. \tag{50}$$

The coherent state (49) is the number projected generalized coherent state of U(3) (see Ref. [4], p. 100, for a definition).

This state lives in the coset space $U(3)/U(2)\otimes U(1)$ and it is often referred as the "projective" state to distinguish it from the "algebraic" state

$$|[N];\eta_x,\eta_y\rangle = e^{\eta_x\tau_x^\dagger\sigma+\eta_x^*\tau_x^\dagger\sigma+\eta_y\tau_y^\dagger\sigma+\eta_y^*\tau_y^\dagger\sigma}(\sigma^\dagger)^N|0\rangle, \quad (51)$$

also called Glauber state in quantum optics. These coherent $U(n)$ states were introduced by Gilmore [7] and others [23–25] in the context of nuclear physics [Lipkin-Meshkov-Glick quasispin model U(2) [26] and Arima-Iachello interacting boson model U(6) [4]] and later in the context of molecular physics [27,28] (Iachello-Levine vibron model U(4) [5]). The coherent states (49) have been recently generalized to excited states [29]. The intrinsic state allows one to associate classical coordinates to any operator defined in terms of the elements of the algebra. It should be noted that the parameters in the coherent state are in general complex and represent coordinates and momenta [28]. For the applications in this paper we consider only the dependence on coordinates, and thus put all momenta p_r, p_θ equal to zero.

1. Energy functional

The ground-state energy functional is the expectation value of the Hamiltonian in the intrinsic state of Eq. (49),

$$E(r,\theta) \equiv \frac{\langle[N];r,\theta|\hat{H}|[N];r,\theta\rangle}{\langle[N];r,\theta|[N];r,\theta\rangle}. \quad (52)$$

By minimizing $E(r,\theta)$ with respect to r and θ, one obtains [19] an approximation to the exact ground-state energy which is good to order $1/N$.

For the evaluation of E in the boson condensate of Eq. (50), it is convenient to rewrite the Hamiltonian in terms of Cartesian boson operators, that is

$$\hat{n} = \tau_x^\dagger\tau_x + \tau_y^\dagger\tau_y,$$

$$\hat{l} = i(\tau_y^\dagger\tau_x - \tau_x^\dagger\tau_y),$$

$$\hat{l}^2 = \hat{n} + 2\tau_y^\dagger\tau_x^\dagger\tau_y\tau_x - (\tau_y^\dagger)^2(\tau_x)^2 - (\tau_x^\dagger)^2(\tau_y)^2,$$

$$\hat{P} = N(N-1) - 2\hat{n}\hat{n}_s - 2\tau_y^\dagger\tau_x^\dagger\tau_x\tau_y + \{(\tau_y^\dagger)^2(\tau_x)^2 - [(\tau_y^\dagger)^2 + (\tau_x^\dagger)^2]\sigma^2 + (\tau_x^\dagger)^2(\tau_y)^2 - [(\sigma^\dagger)^2(\tau_y)^2 + (\tau_x)^2]\}. \quad (53)$$

The ground-state energy functional for the two-body general Hamiltonian of Eq. (15) is

$$E(r) = E_0 + \epsilon N\frac{r^2}{1+r^2} + \alpha\left(N(N-1)\frac{r^2}{1+r^2} + 2N\right)\frac{r^2}{1+r^2} + \beta N\frac{r^2}{1+r^2} + AN(N-1)\left(\frac{1-r^2}{1+r^2}\right)^2. \quad (54)$$

This energy functional does not depend on θ, since the Hamiltonian is a scalar operator. The energy functional for the essential Hamiltonian (44) is trivially obtained from Eq. (54). The energy per particle $\mathcal{E}=E/N$ is

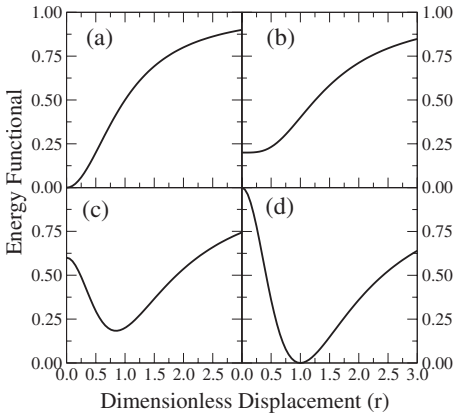

FIG. 8. Energy functional, Eq. (55), for four different values of ξ spanning the range of possible physical situations ranging from (a) rigidly linear (ξ=0.0), (b) quasilinear (ξ=0.2), (c) quasibent (ξ=0.6), and (d) rigidly bent (ξ=1.0).

$$\mathcal{E}_\xi(r) = \epsilon\left[(1-\xi)\frac{r^2}{1+r^2} + \xi\left(\frac{1-r^2}{1+r^2}\right)^2\right], \quad (55)$$

where ϵ is an overall scale and ξ is the control parameter. The differences between the four regimes discussed above can now be understood by comparing with the associated energy functionals depicted in Fig. 8. In this figure, the panels include the energy functional for ξ=0, 0.2, 0.6, and 1, which represents the rigidly linear, quasilinear, quasibent, and rigidly bent situations, respectively. The ξ=0 case has a sharp minimum at the origin. The flatness of the potential increases with ξ, being maximum for ξ=0.2. For values greater than 0.2 a hump at the origin appears, while for ξ =1 there is an absolute maximum at the origin and a sharp minimum at r=1. For application to linear-to-bent transitions in molecules, it has become customary to plot the energy functional (also called the "potential") not as a function of the displacement r but as a function of the bending angle $\phi=r/a$ where a is the bond length and to allow both positive and negative values of ϕ as shown in Fig. 9.

2. Classical limit of other operators of interest

The intrinsic state formalism can be applied to any operator of interest, not only to the Hamiltonian. An operator of interest is the $\hat{Q}\cdot\hat{Q}$ operator defined in Eq. (41),

$$\hat{Q}\cdot\hat{Q} = \hat{Q}_+\hat{Q}_- + \hat{Q}_-\hat{Q}_+. \quad (56)$$

This operator does not depend on the scalar boson σ but only on the $\tau_\pm$ circular boson operators

$$\hat{Q}\cdot\hat{Q} = 2(\hat{n} + 2\tau_+^\dagger\tau_-^\dagger\tau_+\tau_-). \quad (57)$$

In order to compute the classical limit of the $\hat{Q}\cdot\hat{Q}$ operator one needs to compute only the expectation value of the second term $\langle[N];r,\theta|\tau_+^\dagger\tau_-^\dagger\tau_+\tau_-|[N];r,\theta\rangle$, where

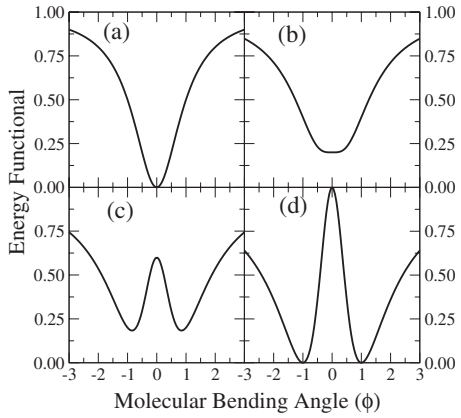

FIG. 9. Energy functional, for linear-to-bent transition in molecules, as a function of the bending angle ϕ for four different values of ξ, (a) rigidly linear (ξ=0.0), (b) quasilinear (ξ=0.2), (c) quasibent (ξ=0.6), and (d) rigidly bent (ξ=1.0), and a=1.

$$\tau_+^\dagger \tau_-^\dagger \tau_+ \tau_- = \frac{1}{4}[(\tau_x^\dagger)^2(\tau_x)^2 + (\tau_x^\dagger)^2(\tau_y)^2 + (\tau_y^\dagger)^2(\tau_x)^2 + (\tau_y^\dagger)^2(\tau_y)^2]. \tag{58}$$

The classical limit of the quadrupole operator is given by

$$\langle [N]; r, \theta | \hat{Q} \cdot \hat{Q} | [N]; r, \theta \rangle = 2N \frac{r^2}{1+r^2} + N(N-1) \frac{r^4}{(1+r^2)^2},$$

and it is again independent of θ.

The classical limit of transition operators is also of interest. The classical limit of the infrared transition operator (45) is

$$\langle [N]; r, \theta | \hat{T}^{\mathrm{IR}}_{\pm} | [N]; r, \theta \rangle = 2t\sqrt{N} \frac{r}{1+r^2} e^{\pm i\theta}. \tag{59}$$

This classical limit depends on θ, since the operator $\hat{T}^{\mathrm{IR}}$ is not a scalar, but a 2D vector.

C. Symmetry breaking and shape phase transitions

Ground-state phase transitions in algebraic models can be studied in several related ways: By analyzing the ground-state energy functional and its derivatives as a function of the control parameter (Ehrenfest criterion); by analyzing the order parameter and its derivatives as a function of the control parameter; by analyzing the behavior of the level densities. In this paper we use, for simplicity, Ehrenfest classification, in which the phase transition is of zeroth order if the energy functional at equilibrium $\mathcal{E}(r=r_e)$ is discontinuous, and of nth order if its nth derivative with respect to ξ is discontinuous [7,8].

The study of phase transitions in the U(3) model is straightforward. Denoting by r_e the equilibrium value we obtain from $d\mathcal{E}_\xi(r)/dr=0$ the equilibrium values

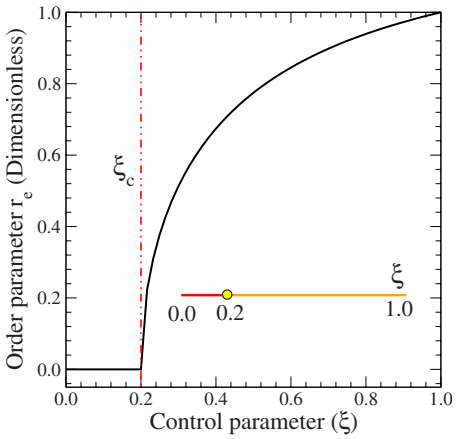

FIG. 10. (Color online) Classical order parameter r_{min} in arbitrary units as a function of the control parameter ξ. A dotted-dashed line indicates the position of the critical value of the control parameter.

$$r_e = 0, \sqrt{\frac{5\xi - 1}{3\xi + 1}}. \tag{60}$$

For $\xi \leq \xi_c$=0.2 the minimum is at the origin, while for values of ξ greater than ξ_c=0.2 the minimum at the origin is replaced by a maximum and a new minimum appears. When evaluated for $r=r_e$, the energy functional is

$$\mathcal{E}_\xi(r_e) = \begin{cases} \xi, & 0 \leq \xi \leq \xi_c, \\ \dfrac{-9\xi^2 + 10\xi - 1}{16\xi}, & \xi_c < \xi \leq 1. \end{cases} \tag{61}$$

By evaluating the derivative of $\mathcal{E}_\xi(r_e)$ with respect to ξ, one finds that the second derivative is discontinuous at $\xi=\xi_c$,

$$\frac{d\mathcal{E}_\xi(r_e)}{d\xi} = \begin{cases} 1, & 0 \leq \xi \leq \xi_c, \\ \dfrac{-9\xi^2 + 1}{16\xi^2}, & \xi_c < \xi \leq 1, \end{cases}$$

$$\frac{d^2\mathcal{E}_\xi(r_e)}{d\xi^2} = \begin{cases} 0, & 0 \leq \xi \leq \xi_c, \\ -\dfrac{1}{8\xi^3}, & \xi_c < \xi \leq 1. \end{cases} \tag{62}$$

The phase transition is then of second order. The classical order parameter can be taken as r_e. The behavior of r_e as a function of ξ, obtained from Eq. (60), is shown in Fig. 10, again displaying a typical behavior of a second-order transition [30]. By writing $r_e \propto (\xi - \xi_c)^\mu$ for $\xi > \xi_c$ and in the neighborhood of ξ_c, one can extract from Eq. (60) the classical critical exponent, $\mu=\frac{1}{2}$. There has been recently considerable interest in critical exponents for phase transitions of the U(n)-SO($n+1$) type [9,31]. It appears that all phase transitions of this type have critical exponent $\frac{1}{2}$. Figure 10 includes, in the inset, the phase diagram for the present system. It is a one-dimensional diagram as we only have one control parameter where the two possible phases (linear or bent) are separated by a critical point at $\xi=\xi_c$=0.2.

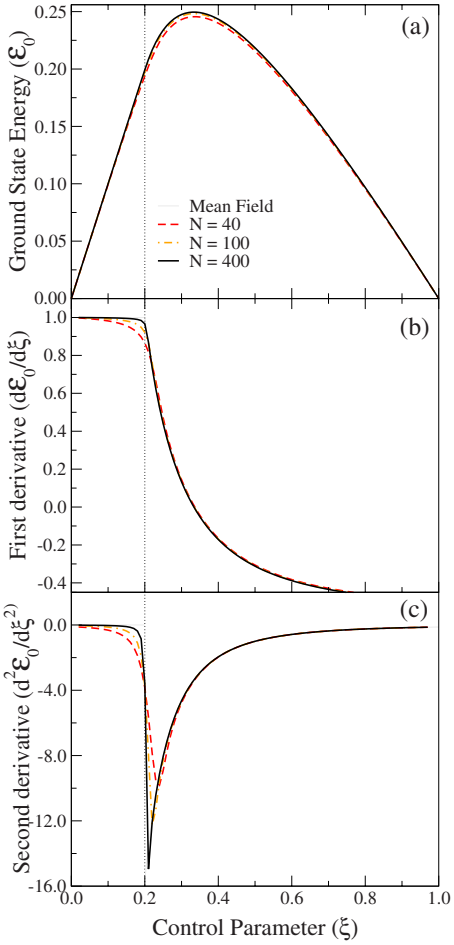

FIG. 11. (Color online) (a) Ground-state energy $\mathcal{E}_0$, (b) its first derivative $\partial\mathcal{E}_0/\partial\xi$, and (c) its second derivative $\partial^2\mathcal{E}_0/\partial\xi^2$ as a function of the control parameter ξ for $N=40,\ 100,\ 400$. The full thin gray line v corresponds to the mean-field result from Eqs. (61) and (62). A vertical dotted line indicates the position of the critical value of the control parameter.

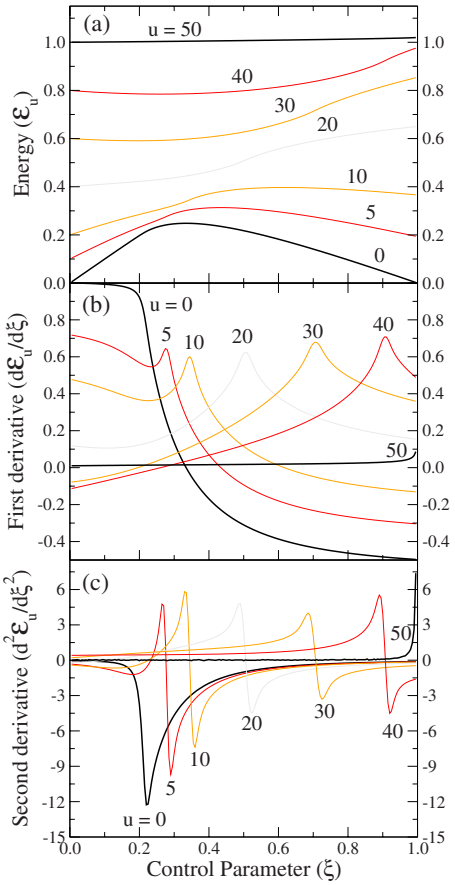

FIG. 12. (Color online) Dependence of the energy [panel (a), in arbitrary units], its first [panel (b)] and second [panel(c)] derivatives with the control parameter, ξ, for eigenstates labelled by u, and $N=100$.

The classical (mean-field) result ($N\to\infty$) can be compared with numerical calculations for finite N. In Fig. 11 we show in panels (a), (b), and (c) the ground-state energy $\mathcal{E}_0(\xi)$, its first $\partial\mathcal{E}_0(\xi)/\partial\xi$, and second derivative $\partial^2\mathcal{E}_0(\xi)/\partial\xi^2$, respectively, computed numerically for $N=40,100,400$. Even for small N values ($N=40$) the mean field provides a good approximation to the exact result except in a narrow region around the critical value $\xi=\xi_c$. Due to the second-order nature of the phase transition that takes place when $\xi=\xi_c$, the first derivative is a continuous function and the second derivative is discontinuous at the critical value of the control parameter. The numerical calculation closely follows this behavior.

We have extended the numerical study of the ground-state energy and its derivatives to excited vibrational states. Labeling the vibrational states by u, as in the preceding section, we plot in Fig. 12 the energy per particle $\mathcal{E}_u$ and its derivatives $\partial\mathcal{E}_u/\partial\xi$ and $\partial^2\mathcal{E}_u/\partial\xi^2$ as a function of ξ. From this figure one can see that the discontinuity in the second derivative, which occurs at $\xi=\xi_c=0.2$ for the ground state $u=0$, moves toward larger values of ξ with increasing u, and reaches $\xi=1$ for the uppermost state, $u=N/2$. The concept of ground-state phase transition (QPT) has been recently extended to excited-state phase transitions (ESQPT) [32]. The numerical results in Fig. 12 are in agreement with the occurrence of excited-state phase transitions in the U(2)-SO(3) transition.

In addition to energies, finite N effects can also be studied for the order parameter. It is convenient to use as quantal order parameter the expectation value of the number operator $\hat{n}$ in the ground state

$$\langle\hat{n}\rangle \equiv \langle u=0|\hat{n}|u=0\rangle. \tag{63}$$

The classical limit for this quantity is

$$\langle[N];r,\theta|\hat{n}|[N];r,\theta\rangle = N\frac{r_e^2}{1+r_e^2}, \tag{64}$$

and it is thus related to the classical order parameter r_e, shown in Fig. 10. In Fig. 13 we show the normalized quantal order parameter $\langle\hat{n}\rangle/N$. As one can see, the quantal order parameter tends to the classical limit as $N\to\infty$.

The same behavior with increasing N values can be found also for the matrix elements of other operators as shown in Fig. 14 for the dipole moment. The normalized results for the transition $|\langle[N];0,0|\hat{T}^{\mathrm{IR}}_{\pm}[N];1,1\rangle|$ tends to the classical limit

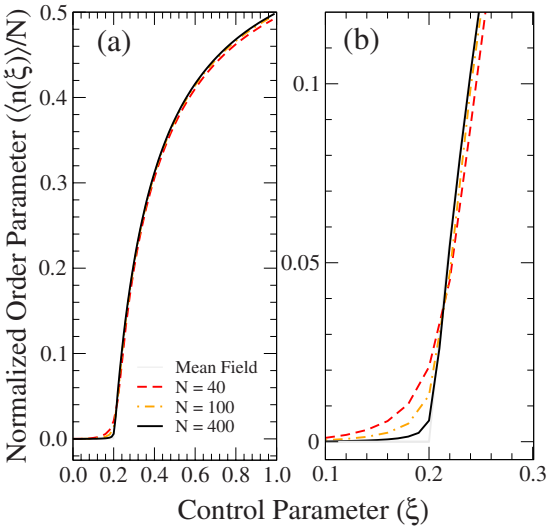

FIG. 13. (Color online) Finite N effects in the normalized order parameter $\langle \hat{n} \rangle / N$. Panel (a) full range of variation of ξ; panel (b) detail of the zone around $\xi_c = 0.2$. The full thin gray line is the mean-field result.

as N increases from $N=40$ to $N=400$. In view of the fact that the dipole function is directly related to the classical order parameter, r_e, measurements of infrared transition rates, Eq. (48), provide the most direct experimental signature for phase transitions.

D. Finite-N scaling behavior

A general theory of finite-size scaling (for a review, see [33]) was formulated years ago by Fisher [34] and Fisher and Barber [35], especially for applications to condensed matter systems. Stimulated by the renewed interest in quantum phase transitions in nuclei and molecules [36] due to the suggestion of a simple scale-invariant behavior for the excitation energies of nuclei at the critical point of shape-phase

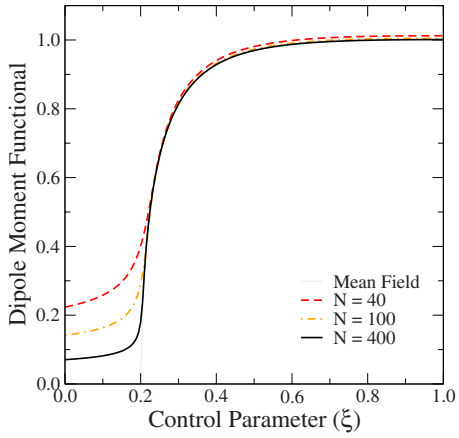

FIG. 14. (Color online) The full thin line is the mean-field limit of the dipole moment functional $\hat{T}^{\mathrm{IR}}_{\pm}$ evaluated at r_e. The calculated values of $|\langle [N];0,0|\hat{T}^{\mathrm{IR}}_{\pm}[N];1,1\rangle|/N$ for $N=40,100,400$ are shown and compared with the mean-field limit.

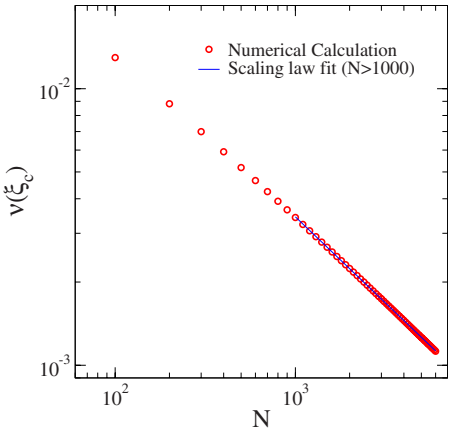

FIG. 15. (Color online) Double logarithm plot of the N dependence of the normalized order parameter $\nu(\xi_c)$.

transitions [37–40], Rowe *et al.* [41] initiated a study of finite-size scaling behavior within the context of algebraic models, in particular the interacting boson model of Arima and Iachello [4]. Finite-size scaling exponents in this model have also been evaluated by Dusuel *et al.* [42,43] by means of the continuous unitary transformation technique and by numerical diagonalization of the U(6) Hamiltonian for the second-order quantum phase transition between the U(5), spherical, and SO(6), deformed phase. Finite-N scaling exponents for the ground-state energy, E_0, the gap, Δ, the number of d bosons in the ground state, $\langle \hat{n}_d \rangle_{\mathrm{gs}}$, and the $B(E2)$ transition probabilities $0^+ \rightarrow 2^+$ were discussed. In this paper we present the numerical determination of the finite-size scaling exponents for several quantities of interest in the U(3) model.

1. Order parameter

We begin by considering the scaling behavior of the normalized order parameter of Fig. 13,

$$\nu(\xi) = \frac{\langle n(\xi) \rangle}{N}. \tag{65}$$

This is the ground-state expectation value of the operator $\hat{n}$ of Eq. (5), that counts the number of bosons in the upper level, $\hat{n} = \hat{n}_+ + \hat{n}_-$, normalized with N. In the limit $N \rightarrow \infty$, we have

$$\nu(\xi) = \begin{cases} 0, & 0 \leq \xi \leq \xi_c, \\ \dfrac{5\xi - 1}{8\xi}, & \xi_c < \xi \leq 1. \end{cases} \tag{66}$$

We have computed numerically this quantity at $\xi = \xi_c$ by exact diagonalization of the Hamiltonian (44) for $N = 100-6000$ and subsequent evaluation of the matrix elements, and fit it with the power law

$$\nu(\xi = \xi_c) = A_{n0} N^{-A_{n1}}. \tag{67}$$

The results are shown in a double logarithm plot in Fig. 15. From the fit to the data points with $N \geq 1000$ we extract

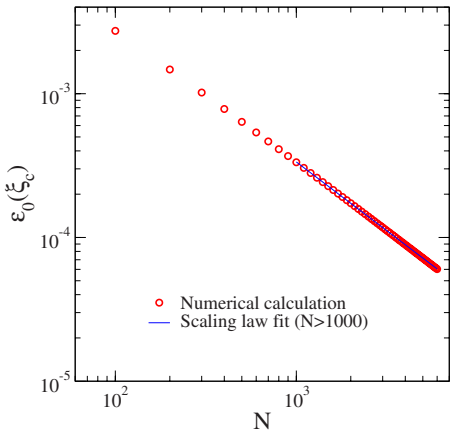

FIG. 16. (Color online) Double logarithm plot of the N dependence of the ground-state energy $\epsilon_0(\xi_c)$.

$A_{n0}=0.2545(4)$ and $A_{n1}=0.6230(5)$, with a suggested asymptotic value of $A_{n1}=\frac{2}{3}$.

2. Ground-state energy

We consider next the ground-state energy. It is convenient to introduce the function

$$\epsilon_0(\xi) = \xi - E_0(\xi), \tag{68}$$

where $E_0(\xi)$ is the ground-state energy for the Hamiltonian (44). We have introduced this function because, in the $N\to\infty$ limit, we have

$$\epsilon_0(\xi) = \begin{cases} 0, & 0 \le \xi \le \xi_c, \\ \dfrac{25\xi^2 - 10\xi + 1}{16\xi}, & \xi_c < \xi \le 1, \end{cases} \tag{69}$$

and it is thus possible to fit the scaling behavior with the simple power law

$$\epsilon_0(\xi = \xi_c) = A_{\epsilon 0} N^{-A_{\epsilon 1}}. \tag{70}$$

The results are given in a double logarithm plot in Fig. 16. From the fit we extract $A_{\epsilon 0}=0.2480(4)$ and $A_{\epsilon 1}=0.9564(5)$ with a suggested asymptotic value $A_{\epsilon 1}=1$.

The results for the order parameter and the ground-state energy are summarized in Table I.

3. Gap

Particularly important are the scaling properties of the energy gap, Γ, between the ground state and the excited states. In Refs. [41–43] the scaling properties of the energy gap between the ground state and the first excited vibrational state with zero angular momentum, called Δ, was studied. Here we extend numerically these studies to the second and third vibrational state and to the first, second, and third rotational state. For vibrational states there are two quantities of importance, the energy gap itself and the value of the control parameter at which the minimum in the excitation energy occurs. We define the vibrational energy gap, $\Gamma_{u,\mathrm{vib}}$, for the uth excited vibrational state ($l=0$) as

TABLE I. Parameters obtained after a linear regression to the exponential form $A_0 N^{-A_1}$ of the order parameter, $\nu(\xi_c)$, and of the ground-state energy, $\epsilon_0(\xi_c)$, from data points with $N=1000-6000$.

		Finite-size exponent	Correlation coefficient
$\nu(\xi_c)$	$A_{n0}=0.2545(4)$	$A_{n1}=0.6230(5)$	−0.99998
$\epsilon_0(\xi_c)$	$A_{\epsilon 0}=0.2480(4)$	$A_{\epsilon 1}=0.9564(5)$	−0.999994

$$\Gamma_{u,\mathrm{vib}} = E_u(\xi_{\min,u}) - E_0(\xi_{\min,u}), \tag{71}$$

where $\xi_{\min,u}$ is the value of the control parameter that minimizes the energy difference between the ground state and the uth vibrational state. The gap goes to zero as $N\to\infty$ [41–43]. We parametrize the N dependence as

$$\Gamma_{\mathrm{vib}} = A_0 N^{-A_1}. \tag{72}$$

We define the second quantity as the difference between $\xi_{\min,u}$ and the critical value ξ_c,

$$\Delta\xi_{u,\mathrm{vib}} = \xi_{\min,u} - \xi_c, \tag{73}$$

and parametrize its scaling behavior as

$$\Delta\xi_{\mathrm{vib}} = B_0 N^{-B_1}. \tag{74}$$

The difference $\Delta\xi_{\mathrm{vib}}$ also goes to zero as $N\to\infty$ [41–43].

The behavior of the energy levels for $u=1,2,3$ is shown in Fig. 17. By fitting the gap $\Gamma_{u,\mathrm{vib}}$ and the difference $\Delta\xi_{u,\mathrm{vib}}$ with functions (72) and (74) we determine the values shown in Table II. The value of $A_1=0.337\,42(10)$ that we extract from $u=1$ is in agreement with the suggestion [41] and analytic determination [42,43] of $A_1=\frac{1}{3}$ for the transition U(5)-SO(6). We confirm the results of [32] that all transitions of the type U(n)-SO($n+1$), here U(2)-SO(3) have the same scaling behavior. We note that since the problem here is in 2D while in the interacting boson model investigated in Refs. [41–43] it is in five dimensions, the dimension of the

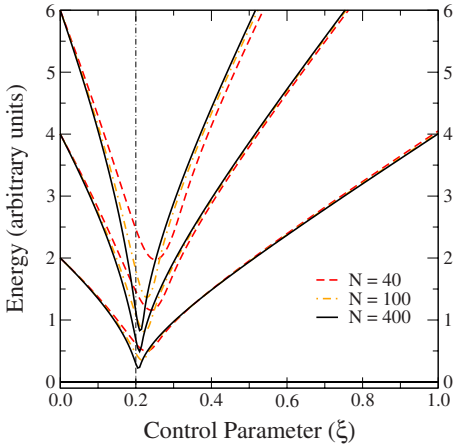

FIG. 17. (Color online) Correlation diagram that shows the vibrational excitation pattern for the first three $l=0$ excited states for $N=40,100,400$. The energy units are arbitrary and the scale $\epsilon=1$. Ground-state energies have been fixed to zero and the critical value of the control parameter $\xi_c=0.2$ has been marked (see text).

TABLE II. Parameters obtained after a linear regression to the exponential forms $A_0N^{-A_1}$ and $B_0N^{-B_1}$ of the vibrational energy gap $\Gamma_{u,\mathrm{vib}}$ and the difference $\Delta\xi_{u,\mathrm{vib}}=\xi_{\min,u}-\xi_c$. The fitted data are shown in Fig. 18. Only $N\geq 500$ data were used as an input for the fit.

		Finite-size exponent	Correlation coefficient
$\Gamma_{1,\mathrm{vib}}$	$A_0=1.62360(17)$	$A_1=0.33743(10)$	−0.999995
$\Gamma_{2,\mathrm{vib}}$	$A_0=3.724(4)$	$A_1=0.33890(13)$	−0.999992
$\Gamma_{3,\mathrm{vib}}$	$A_0=6.265(8)$	$A_1=0.34038(16)$	−0.999990
$\Delta\xi_{1,\mathrm{vib}}$	$B_0=0.3622(19)$	$B_1=0.6544(6)$	−0.99995
$\Delta\xi_{2,\mathrm{vib}}$	$B_0=0.5040(19)$	$B_1=0.6592(5)$	−0.99997
$\Delta\xi_{3,\mathrm{vib}}$	$B_0=0.6160(15)$	$B_1=0.6591(3)$	−0.999990

basis for a given N is considerably smaller here than in the interacting boson model and we are therefore able to follow the scaling behavior up to $N=6000$, as shown in Figs. 18 and 20. Our numerical study of the scaling behavior is thus directly applicable to mesoscopic systems with numbers of particles of the order 10^3-10^4 [44].

In addition to the vibrational behavior, we have investigated the rotational behavior. For the Hamiltonian (44), rotational energies are also expected to collapse to zero energy at the critical value $\xi_c=0.2$ and indeed they do so as it can be seen in Fig. 19. In order to investigate the scaling behavior of rotational excitations we introduce the rotational gap

$$\Gamma_{l,\mathrm{rot}}=E_l(\xi_c)-E_0(\xi_c), \tag{75}$$

of the lth excited state ($u=0$). By fitting the gap with the function

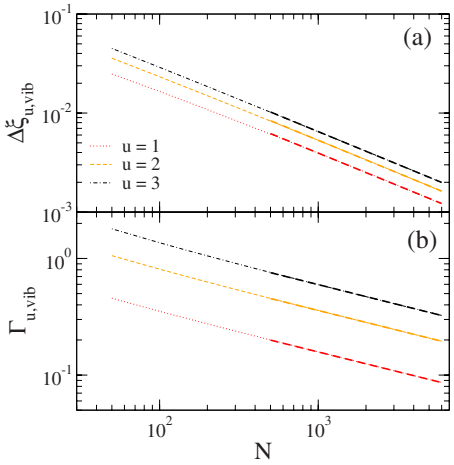

FIG. 18. (Color online) Double logarithm plot of the N dependence of $\Delta\xi_{u,\mathrm{vib}}$, panel (a), and of $\Gamma_{u,\mathrm{vib}}$, panel (b). These quantities are defined in Eqs. (73) and (71), respectively. The numerical calculation results are depicted with a dotted line, a dashed line, and a dotted-dashed line for $u=1$, 2, 3, respectively. The fit to a power law was performed using the numerical results for $N=500-6000$ and the result is depicted using thicker dashed lines in the plot.

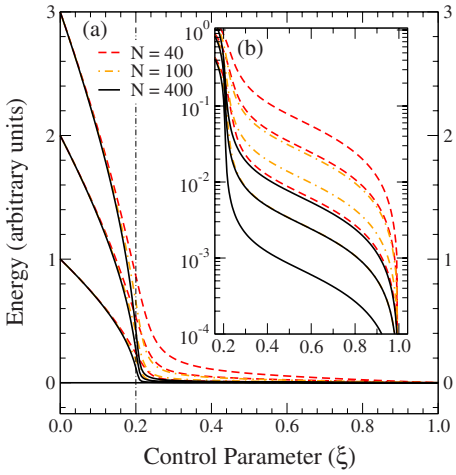

FIG. 19. (Color online) Panel (a), correlation energy diagram that shows the rotational excitation pattern for the $l=1$, 2, and 3 states of the lowest $u=0$ band and $N=40,100,400$. The energy units are arbitrary and the scale $\epsilon=1$. Ground-state $l=0$ energies have been set to zero and the critical value of the control parameter $\xi_c=0.2$ has been marked with a vertical dotted-dashed line. Panel (b) depicts the behavior for $\xi>0.2$ in logarithmic scale.

$$\Gamma_{\mathrm{rot}}=C_0N^{-C_1}, \tag{76}$$

we determine the values shown in Table III. The value we obtain, $C_1=0.317\,21(11)$, suggests that Γ_{rot} scales as Γ_{vib}, with scaling coefficient $\frac{1}{3}$.

The numerical study presented in this section complements the analytical determination of the finite-size scaling exponents done recently by one of the authors with Caprio and Cejnar [32] for a large class of two level algebraic models, including the U(3) vibron model discussed here. In particular, it supports the value $\frac{1}{3}$ for the scaling exponent A_1 of

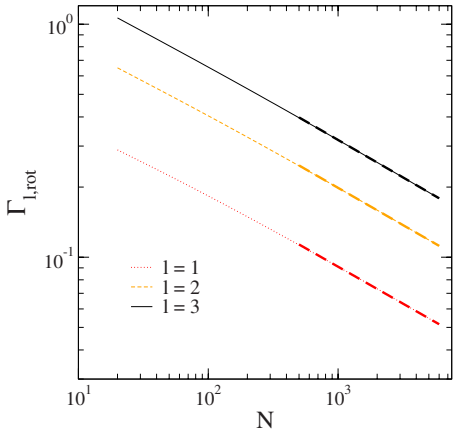

FIG. 20. (Color online) Double logarithm plot showing the variation with N of the rotational energy gap, $\Gamma_{l,\mathrm{rot}}$, defined in Eq. (75), for $l=1,2,3$. The numerical calculation results are depicted with a dotted (red) line, a dashed (orange) line, and a full (black) line for $l=1$, 2, and 3, respectively. The fit to a power law was performed using the numerical results for $N=500-6000$ and the result is depicted using thicker dashed lines in the plot.

TABLE III. Parameters obtained after a linear regression to the exponential forms $C_0N^{-C_1}$ of the rotational energy gaps, $\Gamma_{l,\mathrm{rot}}$. The fitted data are shown in Fig. 20. Only $N \geq 500$ data were used as an input for the fit.

		Finite-size exponent	Correlation coefficient
$\Gamma_{1,\mathrm{rot}}$	$C_0=0.81455(9)$	$C_1=0.31721(11)$	−0.99998
$\Gamma_{2,\mathrm{rot}}$	$C_0=1.8081(12)$	$C_1=0.31984(9)$	−0.999990
$\Gamma_{3,\mathrm{rot}}$	$C_0=2.9375(17)$	$C_1=0.32160(5)$	−0.999993

the vibrational gap Γ_1, numerically determined to be 0.337 43(10).

IV. MONODROMY IN THE U(3) APPROACH

We consider once more the behavior of the excited-state energies as a function of ξ (correlation diagram) for U(2)-SO(3), shown in Fig. 21 for $N=40$ and $l=0$. We see in this diagram a separatrix between states with U(2) character (left-hand side) and SO(3) character (right-hand side) denoted by a dashed line. The equation of the separatrix for $N \to \infty$ is

$$f(\xi) = \frac{25\xi^2 - 10\xi + 1}{16\xi}. \tag{77}$$

For finite N and normalization as in Eq. (44), $f(\xi)$ should be multiplied by a factor $(N+1)/(N-1)$. The change in character of the states as one crosses the separatrix is further illustrated in Fig. 22, called a "quantum monodromy diagram" [14]. One can see from this diagram that vibrational states with $u > u_m$, where u_m is the value of u at which the separatrix is crossed for fixed ξ, have a quadratic rotational behavior

$$E(l) = E_0 + al^2, \quad u < u_m, \tag{78}$$

as in SO(3), while for $u > u_m$ have linear behavior

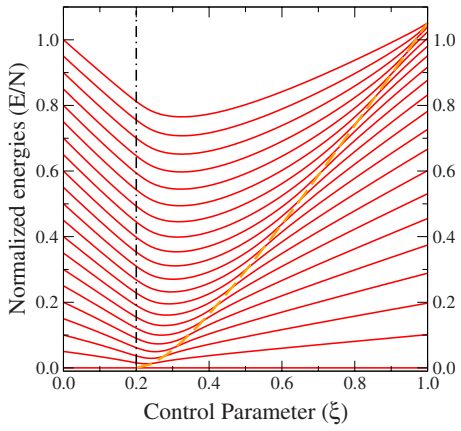

FIG. 21. (Color online) Correlation diagram for $N=40$ and vibrational angular momentum $l=0$. The normalized energy values E/N are plotted against ξ as full (red) lines. The critical point $\xi_c = 0.2$ is marked with a vertical dotted-dashed line. The separatrix, Eq. (77), for $N=40$ is shown with a dashed (orange) line.

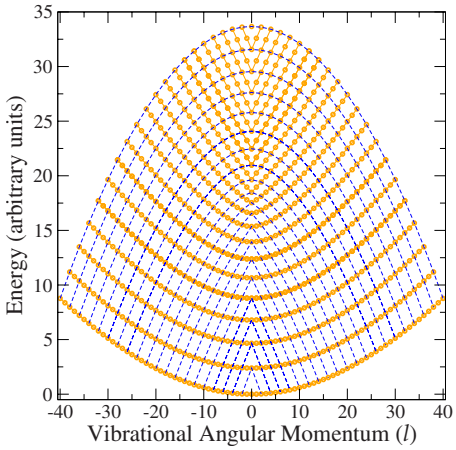

FIG. 22. (Color online) Energy spectrum for $N=40$ and $\xi=0.6$ as a function of the vibrational angular momentum l. Points linked by full (orange) lines correspond to the same value of v, while points joined by dashed (blue) lines correspond to the same value of n. In the last case, for sake of clarity, only points with even values of n have been connected. In both cases, one can see the transition from smooth to warped variations at $l=0$ when crossing the monodromy region.

$$E(l) = E_0 + bl, \quad u > u_m, \tag{79}$$

as in U(2).

The change in character of the states as one crosses the separatrix can be also easily understood by considering the potential energy functional, Eq. (55), which can be rewritten as

$$V_{\mathrm{alg}}(r) = a\frac{r^2}{1+r^2} + b\frac{r^4}{(1+r^2)^2}. \tag{80}$$

For values of $\xi > \xi_c$ the potential has a hump at the origin, see, for example, panel (c) of Figs. 8 and 9. The quantum states of the potential (c) change in character when going from below to above the maximum. The states at energies close to the potential hump have special properties, which can be associated to the concept of monodromy [14], hence the name monodromy plot given to Fig. 22. We note also that the study of monodromy is usually done on the quartic potential

$$V(r) = ar^2 + br^4. \tag{81}$$

The difference between the monodromy plot of Fig. 22 and that obtained from the quartic potential is that the potential (80) has a finite number of bound states (finite number of states in Fig. 22), while the potential (81) has an infinite number of bound states.

An important question in applications of algebraic models to physical systems is the extent to which features of the calculated spectrum can be observed. As one can see from Fig. 21, the monodromy effect, i.e., an accumulation of energy levels around the separatrix (infinite level density for $N \to \infty$), occurs for $\xi > \xi_c$ and at excitation energies which are larger and larger as ξ increases. Also the finiteness of the system smoothes out the infinite level density. It has thus

been difficult to detect experimentally monodromy effects. However, monodromy effects have been very recently observed in the bending vibrational spectra of some molecules [17,45], most notably water [18]. This molecule has been analyzed within the framework of potential models. An analysis within the framework of the U(3) algebra will be presented elsewhere [46].

Monodromy is a well-known topological concept that has been applied to double well potentials in the particular sense of inexistence of a valid set of quantum labels for the full spectrum [14,47–49]. Here we only emphasize that monodromy effects are a typical feature of all algebraic models of the U(n)-SO($n+1$) type and that indeed have been analyzed in Refs. [50–52] for the interacting boson model U(5)-SO(6) transition. A connection with ESQPT is given in [32]. Monodromy within the context of this paper is only a term used to make connection with potential models of molecules [14,53]. It should be more properly referred to as properties of excited states in the quasibent region $\xi > \xi_c = 0.2$.

V. THERMODYNAMIC QUANTITIES

The shape phase transitions discussed in the preceding sections occur at zero temperature, $T=0$ K, as a function of the control parameter ξ in the Hamiltonian, Eq. (44). There is a considerable interest on how to extend ground-state phase transitions to excited-state phase transitions and then to introduce temperature (or excitation energy) in algebraic models. A recent attempt is described in Ref. [32]. Here we are interested in studying how the ground-state phase transition affects the thermodynamic quantities and how these quantities are related to spectroscopic properties. We use therefore the simpler (and traditional) method of evaluating the level density and partition function by summing numerically the contributions of each individual state. This method, mostly in the harmonic limit, was used years ago [54], but it has been used recently for anharmonic situations within the context of algebraic approaches [55–57]. In the problem discussed here there are two quantum numbers, u, labeling the vibrational states $u=0,1,2,\ldots,u_{\max}$ and $l=0,\pm 1,\pm 2,\ldots,\pm l_{\max}$, labeling the rotational states. In the infinite system $N\to\infty$, $u_{\max}\to\infty$, and $l_{\max}\to\pm\infty$. For finite N, the partition function can be written as

$$Z(\xi,T)=\sum_{l=0}^{l_{\max}}\sum_{u=0}^{u_{\max}} g_{l,u}\exp\left(-\frac{\eta_{l,u}}{\tau}\right), \tag{82}$$

where $\eta_{l,u}=e_{l,u}/\epsilon$ is the rescaled energy, $\tau=kT/\epsilon$ the reduced temperature, and $g_{l,u}$ the state degeneracy. The values of $u_{\max}$ and $l_{\max}$ are given in Sec. III A, $u_{\max}=\frac{N-1}{2}$ or $\frac{N}{2}$ (N odd or even), $l_{\max}$ for each u being given by the rules of Sec. II B. In order to elucidate the situation, we consider first the contribution of the vibrational motion ($l=0$) for which there is no degeneracy ($g_{0,u}=1$). The $l=0$ partition function as a function of τ for $N=100$ and $\xi=0,0.2,0.6,1$ is shown in panel (a) of Fig. 23, while the dependence on the control parameter ξ for $\tau=0,1,2$ and the same N value is depicted in panel (b) of Fig. 23.

Although the partition function is of no interest in practice, we have plotted it in order to emphasize its behavior as a function of the control parameter ξ, with a maximum in the vicinity of $\xi_c=0.2$, the critical value of ξ. The value at the maximum increases as the reduced temperature increases. The partition function is calculated numerically by inserting in Eq. (82) the energies obtained by diagonalization of the Hamiltonian, Eq. (44), for each value of ξ.

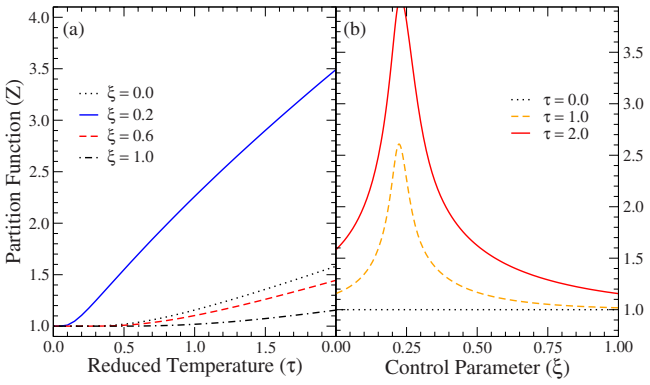

FIG. 23. (Color online) Panel (a), vibrational partition function Z ($l=0$) as a function of the reduced temperature τ for $\xi=0.0,0.2,0.6,1.0$ and $N=100$. Panel (b), partition function Z ($l=0$) as a function of the control parameter ξ for $\tau=0.0,1.0,2.0$ and $N=100$.

Once the partition function is known, other thermodynamic quantities can be calculated. For example, the heat capacity C_p is given by

$$\gamma(\xi,\tau)=\frac{C_p}{R}=\frac{d}{d\tau}\left(\tau^2\frac{d}{d\tau}(\ln Z)\right). \tag{83}$$

The dependence on τ and ξ of the purely vibrational heat capacity is shown in panels (a) and (b) of Fig. 24, respectively, for $N=100$. Note in panel (b) of Fig. 24, the sharp variation of the heat capacities at values around ξ_c.

The contribution of the rotational motion ($l\neq 0$) can be calculated in a similar way. In order to understand whether or not these features of the heat capacity can be measured we plot in Fig. 25 the predicted heat capacity of the bending

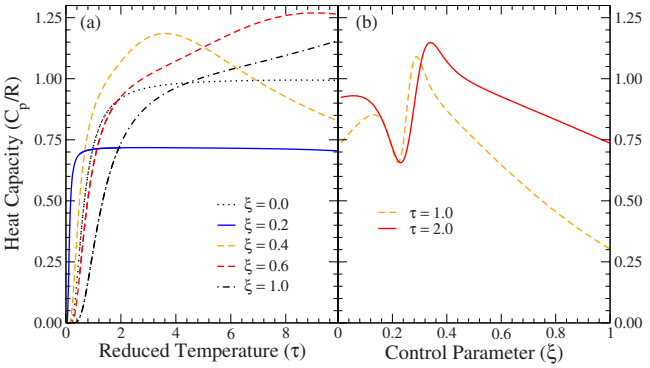

FIG. 24. (Color online) Panel (a), heat capacity $\gamma=C_p/R$ as a function of the reduced temperature τ for $\xi=0.0,0.2,0.4,0.6,1.0$ and $N=100$. Panel (b), heat capacity $\gamma=C_p/R$ as a function of the control parameter ξ for $\tau=1.0,2.0$ and $N=100$.

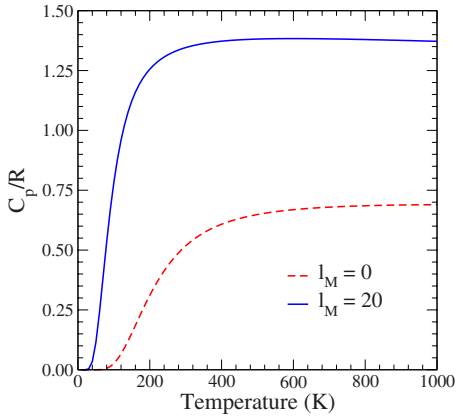

FIG. 25. (Color online) Heat capacity $\gamma=C_p/R$ associated to the H-C-NO bending degree of freedom (ν_5) of fulminic acid (HCNO). The dashed (red) line corresponds to the purely vibrational calculation, $l=0$, while the full (blue) line combines vibrations and rotations up to $l_M=20$, where convergence in calculations occurs for the considered temperature interval.

vibration of HCNO (fulminic acid). This heat capacity has been calculated by first fitting the experimental data with a model Hamiltonian with $\xi=0.1915(15)$ and scale parameter $\epsilon=597(4)$ cm^{-1} [15], inserting the energies into Eq. (82) and numerically evaluating C_p/R. We note that the temperature associated with the scale parameter is $T_\epsilon=859$ K, while the temperature associated to the bending fundamental vibration ($u=1$, $l=\pm 1$) with energy 224.1 cm^{-1} is 156 K. One can see from Fig. 25 that the large jump in C_p/R occurs at temperatures of the order of 120 K when the rotational contribution is included and thus at temperatures that can in principle be obtained although with some difficulty.

VI. CONCLUSIONS

In this paper we have investigated the U(2)-SO(3) phase transition that occurs in the U(3) algebraic approach to 2D systems and applied our results to the study of linear-bent transitions in molecules. We have shown that the phase transition is second order in the $N\to\infty$ limit and investigated numerically the scaling behavior of various quantities. Particularly relevant is the scaling behavior of the energy gap for vibrational excitations, $\Gamma_{\rm vib}$. We have confirmed that the gap goes to zero as $\Gamma_{\rm vib}\sim N^{-1/3}$. We have also studied the energy gap for rotational excitations, $\Gamma_{\rm rot}$, and shown that this too goes to zero. The U(2)-SO(3) phase transition has four distinct regions which, when describing bending vibrations of molecules can be characterized as rigidly linear, quasilinear, quasibent, and rigidly bent. We have discussed the properties of these regions and found that the quasibent region ($0.2<\xi<1$) has unusual properties with anharmonicities shifting from positive to negative and rotational spectra shifting from quadratic to linear at higher energies. These unusual properties arise from the occurrence of a hump at the origin in the energy functional and can be associated with the concept of monodromy. Finally we have calculated the heat capacity of bending vibrations and found that this too has

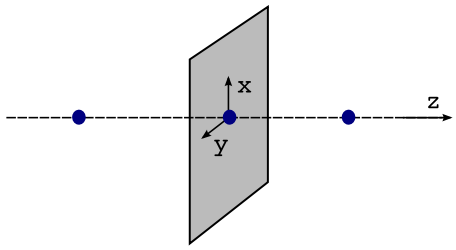

FIG. 26. (Color online) Choice of coordinates for the study of bending vibrations in a triatomic molecule. The axis x and y is in the plane perpendicular to the molecular axis, which is parallel to the z axis.

unusual features at the critical value of the phase transition, a consequence of the vanishing of the gap and of the divergence of the partition function. Both of these unusual features can be actually observed in molecules, since as shown in Ref. [45], several molecules can be found which are in the transitional quasilinear or quasibent region. Since, for bending vibrations, typical values for N are $N\sim 150$ [5,15], the correlation energy diagram with this value of N shows that, in molecules with $\xi\sim 0.3-0.4$, monodromy appears at relatively small values of $u_m\sim 5-10$. These values are accessible to experiment. Indeed, in water, H_2O, $u_m=8$ [18]. For molecular species with $\xi\sim 0.2$, the jump in the vibrational heat capacity occurs at temperatures which are experimentally obtainable. The 2D algebraic model is the simplest (nontrivial) model for which all features (critical behavior, monodromy, thermodynamic quantities) can be calculated for both vibrational and rotational excitations, and which can be tested experimentally.

ACKNOWLEDGMENTS

This work was performed in part under DOE Grant No. DE-FG-02-91ER40608. One of the authors (F.P.B.) wishes to thank the ECT (Trento, Italy), where part of this work was carried out. The authors thank Mark Caprio, Pavel Cejnar, José Enrique García-Ramos, and Patrick H. Vaccaro for valuable comments.

APPENDIX A: CIRCULAR BOSONS AND CARTESIAN BOSONS

In this paper we are interested in applications of the 2D algebraic approach to bending vibrations of molecules. These vibrations occur on a plane. We denote the coordinates in the plane by x and y, with z being the molecular axis as it is schematically depicted in Fig. 26. The coordinates x,y and their derivatives $\partial/\partial x,\partial/\partial y$ transform under a rotation by an angle γ around the z axis as

$$\begin{bmatrix} x' \\ y' \end{bmatrix} = \begin{bmatrix} \cos\gamma & -\sin\gamma \\ \sin\gamma & \cos\gamma \end{bmatrix} \begin{bmatrix} x \\ y \end{bmatrix}, \tag{A1}$$

$$\begin{bmatrix} \frac{\partial}{\partial x'} \\ \frac{\partial}{\partial y'} \end{bmatrix} = \begin{bmatrix} \cos\gamma & -\sin\gamma \\ \sin\gamma & \cos\gamma \end{bmatrix} \begin{bmatrix} \frac{\partial}{\partial x} \\ \frac{\partial}{\partial y} \end{bmatrix}. \tag{A2}$$

The spherical tensor components of the coordinates

$$r_{\pm 1} = \mp \frac{x \pm iy}{\sqrt{2}}, \tag{A3}$$

transform under rotations as $r'_{\pm 1} = \exp(\pm i\gamma) r_{\pm 1}$. We next define creation and annihilation operators in the usual way

$$\tau_x^\dagger = \frac{x - \partial/\partial x}{\sqrt{2}}, \quad \tau_x = \frac{x + \partial/\partial x}{\sqrt{2}}, \tag{A4a}$$

$$\tau_y^\dagger = \frac{y - \partial/\partial y}{\sqrt{2}}, \quad \tau_y = \frac{y + \partial/\partial y}{\sqrt{2}}. \tag{A4b}$$

These boson creation and annihilation operators transform according to Eqs. (A1) and (A2). From these we can construct circular boson operators as in Eq. (2a) and (2b). The behavior of the creation operators under rotation of an angle γ around the z axis, $\mathcal{R}(\gamma)$ is

$$\mathcal{R}\tau_+^\dagger\mathcal{R}^{-1} = -\frac{\mathcal{R}\tau_x^\dagger\mathcal{R}^{-1} + i\mathcal{R}\tau_y^\dagger\mathcal{R}^{-1}}{\sqrt{2}} = \exp(i\gamma)\tau_+^\dagger, \tag{A5a}$$

$$\mathcal{R}\tau_-^\dagger\mathcal{R}^{-1} = \frac{\mathcal{R}\tau_x^\dagger\mathcal{R}^{-1} - i\mathcal{R}\tau_y^\dagger\mathcal{R}^{-1}}{\sqrt{2}} = \exp(-i\gamma)\tau_-^\dagger, \tag{A5b}$$

The Hermitian conjugates, annihilation operators, transform as

$$\mathcal{R}\tau_+\mathcal{R}^{-1} = -\frac{\mathcal{R}\tau_x\mathcal{R}^{-1} - i\mathcal{R}\tau_y\mathcal{R}^{-1}}{\sqrt{2}} = \exp(-i\gamma)\tau_+, \tag{A6a}$$

$$\mathcal{R}\tau_-\mathcal{R}^{-1} = \frac{\mathcal{R}\tau_x\mathcal{R}^{-1} + i\mathcal{R}\tau_y\mathcal{R}^{-1}}{\sqrt{2}} = \exp(i\gamma)\tau_-^\dagger. \tag{A6b}$$

This is not the same as Eq. (A5) but this inconvenience can be overcome with the introduction of $\tilde{\tau}_\alpha$ operators defined as $\tilde{\tau}_\pm = \tau_\mp$. The operators $\tilde{\tau}$ satisfy the equation $\tilde{\tau}_m = (-1)^{1-m}\tau_m$.

APPENDIX B: TRANSFORMATION BRACKETS

Transformation brackets for U(n)-SO($n+1$) can be obtained in a variety of ways. In the interacting boson model they were given in Ref. [58] for the highest weight state. A generic formula for $n \geq 2$ was derived in [59]. We use here a different method, based on a differential realization of the algebra in terms of coordinates and their derivatives [6]. There are two possible SO(3) subalgebras of U(3), one composed of elements $\{\hat{l}, \hat{D}_+, \hat{D}_-\}$, and another composed of $\{\hat{l}, \hat{R}_+, \hat{R}_-\}$, denoted by $\overline{\mathrm{SO(3)}}$.

In order to treat both simultaneously, we introduce operators

$$\hat{O}_+(\alpha) = \sqrt{2}(\tau_+^\dagger\sigma + e^{i\alpha}\sigma^\dagger\tau_-), \tag{B1a}$$

$$\hat{O}_-(\alpha) = \sqrt{2}(e^{-i\alpha}\tau_-^\dagger\sigma + \sigma^\dagger\tau_+). \tag{B1b}$$

The phase $e^{i\alpha}$ arises from an automorphism of the Lie algebra SO(3). We have

$$\hat{R}_+ = \hat{O}_+(0), \quad \hat{R}_- = \hat{O}_-(0), \tag{B2a}$$

$$\hat{D}_+ = \hat{O}_+(\pi), \quad \hat{D}_- = \hat{O}_-(\pi). \tag{B2b}$$

Writing the creation and annihilation operators in terms of coordinates x, y, and a fictitious coordinate s we have

$$\tau_+^\dagger = \frac{1}{2}\left[-x + \frac{\partial}{\partial x} + i\left(-y + \frac{\partial}{\partial y}\right)\right], \tag{B3a}$$

$$\tau_- = \frac{1}{2}\left[x + \frac{\partial}{\partial x} + i\left(y + \frac{\partial}{\partial y}\right)\right], \tag{B3b}$$

$$\sigma^\dagger = \frac{1}{\sqrt{2}}\left(s - \frac{\partial}{\partial s}\right), \tag{B3c}$$

and from these

$$\hat{R}_+ = x\frac{\partial}{\partial s} + s\frac{\partial}{\partial x} + is\frac{\partial}{\partial y} - iy\frac{\partial}{\partial s}, \tag{B4a}$$

$$\hat{D}_+ = xs - iys + \frac{\partial^2}{\partial x\,\partial s} + i\frac{\partial^2}{\partial y\,\partial s}. \tag{B4b}$$

Consider now the algebra $\overline{\mathrm{SO(3)}}$. Using the isomorphism of the algebras $\overline{\mathrm{SO(3)}}$ and SO(3) with the usual angular momentum algebra $\{L_z, L_+, L_-\}$ it is relatively easy to construct the simultaneous eigenfunctions of the operators $\hat{N}$, $\hat{R}^2$, and $\hat{l}$,

$$\hat{N}|[N];\omega,l\rangle = N|[N];\omega,l\rangle, \tag{B5a}$$

$$\hat{R}^2|[N];\omega,l\rangle = \omega(\omega+1)|[N];\omega,l\rangle, \tag{B5b}$$

$$\hat{l}|[N];\omega,l\rangle = l|[N];\omega,l\rangle. \tag{B5c}$$

When written in terms of coordinates, the operator $\hat{N}$ is

$$\begin{aligned}\hat{N} &= \hat{n} + \hat{n}_s = \tau_+^\dagger\tau_+ + \tau_-^\dagger\tau_- + \sigma^\dagger\sigma \\ &= \frac{1}{2}\left(x^2 + y^2 + s^2 - 3 - \frac{\partial^2}{\partial x^2} - \frac{\partial^2}{\partial y^2} - \frac{\partial^2}{\partial s^2}\right) \\ &= \frac{1}{2}\left[r^2 - 3 - \frac{\hat{L}^2}{r^2} - \frac{1}{r^2} - \frac{\partial}{\partial r}\left(r^2\frac{\partial}{\partial r}\right)\right],\end{aligned} \tag{B6}$$

where $r^2 = x^2 + y^2 + s^2$. The eigenfunctions can be split into a radial part and an angular part, $\psi_{\omega,l}^{(N)}(r,\theta,\phi) = f_\omega^{(N)}(r)Y_{\omega l}(\theta,\phi)$, where θ and ϕ are angles in the three-dimensional space spanned by $\{x,y,s\}$. The radial part is the

solution of a three-dimensional harmonic oscillator

$$f_{\omega}^{(N)}(r) = A_{N\omega} r^{\omega} L_{N-\omega/2}^{(\omega+1/2)}(r^2) e^{-r^2/2}, \tag{B7}$$

with the normalization constant $A_{N\omega}$,

$$A_{N\omega} = \sqrt{\frac{2^{2+\omega}(N-\omega)!!}{\sqrt{\pi}(N+\omega+1)!!}}. \tag{B8}$$

The eigenfunctions $\psi_{\omega,l}^{(N)}(r,\theta,\phi)$ can be converted back to the creation-annihilation operator form by the formal substitutions provided by Dragt's theorem,

$$x_{\pm 1} \to \frac{\tau_{\pm}^{\dagger}}{\sqrt{2}}, \quad s \to \frac{\sigma^{\dagger}}{\sqrt{2}},$$

$$\frac{e^{-r^2/2}}{\pi^{3/4}} \to |0\rangle,$$

$$r = \sqrt{x^2+y^2+s^2} \to \sqrt{-\tau_{+}^{\dagger}\tau_{-}^{\dagger} + \frac{\sigma^{\dagger 2}}{2}},$$

$$\cos(\theta) = \frac{s}{r} \to \frac{\sigma^{\dagger}}{\sqrt{-2\tau_{+}^{\dagger}\tau_{-}^{\dagger} + \sigma^{\dagger 2}}},$$

$$e^{\pm i\phi} = \cos(\phi) \pm i\sin(\phi) = \mp \frac{\sqrt{2}x_{\pm 1}}{\sqrt{x^2+y^2}} \to \mp \frac{\tau_{\pm}^{\dagger}}{\sqrt{-\tau_{+}^{\dagger}\tau_{-}^{\dagger}}}. \tag{B9}$$

Making use of the substitutions in Eq. (B9), the highest-weight state with $N=\omega$, $\psi_{\omega,l}^{(\omega)}(r,\theta,\phi)$, can be written as

$$\psi_{\omega,l}^{(\omega)}(r,\theta,\phi) \to |[N=\omega];\omega,l\rangle = \sqrt{\frac{4\pi}{(2\omega+1)!!}} \mathcal{Y}_{\omega l}(\tau^{\dagger},\sigma^{\dagger})|0\rangle, \tag{B10}$$

where $\mathcal{Y}_{\omega l}(\theta,\phi) = r^{\omega} Y_{\omega l}(\theta,\phi)$ is the solid spherical harmonics. A general state $|[N];\omega,l\rangle$ can be obtained from (B10) by applying powers of the scalar operator $-2\tau_{+}^{\dagger}\tau_{-}^{\dagger} + \sigma^{\dagger 2}$, with result

$$|[N];\omega,l\rangle = B_{N\omega}(-2\tau_{+}^{\dagger}\tau_{-}^{\dagger} + \sigma^{\dagger 2})^{N-\omega/2} \mathcal{Y}_{\omega l}(\tau^{\dagger},\sigma^{\dagger})|0\rangle, \tag{B11a}$$

$$B_{N\omega} = (-1)^{N-\omega/2} \sqrt{\frac{4\pi}{(N-\omega)!!(N+\omega+1)!!}}. \tag{B11b}$$

Note that the ill-defined square-root operators disappear from the final form, Eq. (B11a).

We can now proceed to compute the transformation brackets $\langle n,l|\omega,l\rangle$ as the overlap of the states (26) and (B11a). In doing so, the following equations are taken into consideration [6,60]:

$$Y_{\omega l}(\theta,\phi) = C_{\omega l} P_{\omega}^{l}[\cos(\theta)] e^{il\phi}, \tag{B12a}$$

$$C_{\omega l} = \sqrt{\frac{(2\omega+1)(\omega-l)!}{4\pi(\omega+l)!}}, \tag{B12b}$$

$$P_{\omega}^{l}(x) = (-1)^{l}(1-x^2)^{l/2}\frac{d^l}{dx^l}P_{\omega}(x), \tag{B12c}$$

$$P_{\omega}(x) = 2^{-\omega}\sum_{m=0}^{(\omega/2)}(-1)^{m}\binom{\omega}{m}\binom{2\omega-2m}{\omega}x^{\omega-2m}. \tag{B12d}$$

Combining appropriately those equations, we can rewrite the SO(3) states in a way that simplifies the calculation of the transformation brackets,

$$|[N];\omega,l\rangle = B_{N\omega}C_{\omega l}2^{l/2-\omega}l!\sum_{m=0}^{(\omega-l/2)}(-1)^{m}\binom{\omega}{m}\binom{2\omega-2m}{\omega} \times \binom{\omega-2m}{l}\sum_{\mu=0}^{(N-\omega+2m/2)}(-2)^{\mu}\binom{\frac{N-\omega+2m}{2}}{\mu} \times (\tau_{+}^{\dagger})^{\mu+l}(\tau_{-}^{\dagger})^{\mu}(\sigma^{\dagger})^{N-2\mu-l}|0\rangle. \tag{B13}$$

Explicit expressions for the normalization constants $B_{N\omega}$ and $C_{\omega l}$ are given in Eqs. (B11b) and (B12b).

The resulting transformation bracket is

$$\langle [N];n,l|[N];\omega,l\rangle = (-1)^{N-\omega+n-l/2}2^{n/2-\omega} \times \sqrt{\frac{(2\omega+1)(\omega-l)!\left(\frac{n+l}{2}\right)!(N-n)!}{(N-\omega)!!(N+\omega+1)!!\left(\frac{n-l}{2}\right)!(\omega+l)!}} \sum_{\substack{m=0 \\ n-l\le N-\omega+2m}}^{(\omega-l/2)} \frac{(-1)^{m}(2\omega-2m)!\left(\frac{N-\omega+2m}{2}\right)!}{(\omega-m)!m!(\omega-2m-l)!\left(\frac{N-\omega-n+l+2m}{2}\right)!}. \tag{B14}$$

The transformation bracket (B14) is between the U(2) and SO(3) basis. For the transformation brackets between U(2) and SO(3) basis we apply the transformation

$$\tau_{\pm}^{\dagger} \to -i\tau_{\pm}^{\dagger}, \quad \tau_{\pm} \to i\tau_{\pm},$$

$$\sigma^{\dagger} \to \sigma^{\dagger}, \quad \sigma \to \sigma, \tag{B15}$$

and obtain

$$\langle [N]; n, l | [N]; \omega, l \rangle_{\mathrm{SO}(3)} = (-i)^{n+\mathrm{mod}(l,2)} \langle [N]; n, l | [N]; \omega, l \rangle_{\overline{\mathrm{SO}(3)}}. \tag{B16}$$

Equation (B11a) can be used to compute matrix elements of operators. For example, when applying the $\sigma^{\dagger}$ operator to Eq. (B11a) we have

$$\sigma^{\dagger} | [N]; \omega, l \rangle = B_{N\sigma} (-2\tau_{+}^{\dagger}\tau_{-}^{\dagger} + \sigma^{\dagger 2})^{N-\omega+1/2} \times \frac{\sigma^{\dagger}}{\sqrt{-2\tau_{+}^{\dagger}\tau_{-}^{\dagger} + \sigma^{\dagger 2}}} \mathcal{Y}_{\omega,l}(\tau^{\dagger}, \sigma^{\dagger}) |0\rangle. \tag{B17}$$

Making use of Eqs. (B9) we can connect this problem to the recurrence relation for solid spherical harmonics

$$\cos(\theta) \mathcal{Y}_{\omega,l}(\theta,\phi) = \sqrt{\frac{(\omega+l)(\omega-l)}{(2\omega+1)(2\omega-1)}} r \mathcal{Y}_{\omega-1 l}(\theta,\phi) + \sqrt{\frac{(\omega+l+1)(\omega-l+1)}{(2\omega+1)(2\omega+3)}} \frac{\mathcal{Y}_{\omega+1 l}(\theta,\phi)}{r}. \tag{B18}$$

Applying this recurrence relation in Eq. (B17), and taking into account that the operator $\hat{l}$ commutes with $\sigma^{\dagger}$, one can calculate the matrix elements $\langle [N_2]; \omega_2, l | \sigma^{\dagger} | [N_1]; \omega_1, l \rangle$. These matrix elements are given in Eq. (31) for the SO(3) basis.

Similarly, in the case of the $\tau_{\pm}^{\dagger}$ operators, we can take into account the relationship

$$x_{\pm 1} = \mp \frac{x \pm iy}{\sqrt{2}} = \mp \sqrt{\frac{4\pi}{3}} \mathcal{Y}_{1\pm 1}(\theta,\phi), \tag{B19}$$

and the solid spherical harmonics product rule

$$\mathcal{Y}_{1\pm 1}(\theta,\phi) \mathcal{Y}_{\omega,l}(\theta,\phi) = -\langle 1 \pm 1 \omega, l | \omega - 1 l \pm 1 \rangle \sqrt{\frac{3\omega}{4\pi(2\omega-1)}} r^2 \mathcal{Y}_{\omega-1 l\pm 1}(\theta,\phi) + \langle 1 \pm 1 \omega, l | \omega + 1 l \pm 1 \rangle \sqrt{\frac{3\omega}{4\pi(2\omega+3)}} \mathcal{Y}_{\omega+1 l\pm 1}(\theta,\phi). \tag{B20}$$

Making the substitution $\tau_{\pm}^{\dagger} \to x_{\pm 1}$, we obtain the matrix elements given in Eq. (34).

[1] F. Iachello, *Contemporary Mathematics* (American Mathematical Society, Providence, RI, 1994), Vol. 160, pp. 151–171.
[2] F. Iachello, Rev. Mod. Phys. **65**, 569 (1993).
[3] F. Iachello, *Lie Algebras and Applications*, Lecture Notes in Physics Vol. 708 (Springer, Berlin, 2006).
[4] F. Iachello and A. Arima, *The Interacting Boson Model* (Cambridge University Press, Cambridge, 1987).
[5] F. Iachello and R. D. Levine, *Algebraic Theory of Molecules* (Oxford University Press, Oxford, 1995).
[6] A. Frank and P. van Isacker, *Algebraic Methods in Molecular and Nuclear Structure Physics* (Wiley, New York, 1994).
[7] R. Gilmore, J. Math. Phys. **20**, 891 (1979).
[8] D. H. Feng, R. Gilmore, and S. R. Deans, Phys. Rev. C **23**, 1254 (1981).
[9] P. Cejnar and F. Iachello, J. Phys. A **40**, 581 (2007).
[10] F. Iachello and S. Oss, J. Chem. Phys. **104**, 6956 (1996).
[11] F. Iachello, Philos. Mag. Lett. **82**, 289 (2002).
[12] F. Pan, Y. Zhang, S. Jin, J. P. Draayer, M.-L. Ge, and J. L. Birman, Phys. Lett. A **341**, 291 (2005).
[13] S. Jin, B. Xie, H. Zhang, J. L. Birman, and M.-L. Ge, Philos. Mag. Lett. **86**, 743 (2006).
[14] M. S. Child, J. Phys. A **31**, 657 (1998).
[15] F. Iachello, F. Pérez-Bernal, and P. H. Vaccaro, Chem. Phys. Lett. **375**, 309 (2003).
[16] F. Pérez-Bernal, L. F. Santos, P. H. Vaccaro, and F. Iachello, Chem. Phys. Lett. **414**, 398 (2005).
[17] B. P. Winnewisser, M. Winnewisser, I. R. Medvedev, M. Behnke, F. C. DeLucia, S. C. Ross, and J. Koput, Phys. Rev. Lett. **95**, 243002 (2005).
[18] N. F. Zobov, S. V. Shirin, O. L. Polyansky, J. Tennyson, P.-F. Coheur, P. F. Bernath, M. Carleer, and R. Colin, Chem. Phys. Lett. **414**, 193 (2005).
[19] R. Gilmore and D. Feng, Nucl. Phys. A. **301**, 189 (1978).
[20] W. R. Thorson and I. Nakagawa, J. Chem. Phys. **33**, 994 (1960).
[21] G. Herzberg, *Molecular Spectra and Molecular Structure, Vol. III: Electronic Spectra and Electronic Structure of Polyatomic Molecules* (Van Nostrand-Reinhold, New York, 1966).
[22] R. N. Dixon, Trans. Faraday Soc. **60**, 1363 (1964).
[23] J. N. Ginocchio and M. W. Kirson, Phys. Rev. Lett. **44**, 1744 (1980).
[24] A. Bohr and B. R. Mottelson, Phys. Scr. **22**, 468 (1980).
[25] A. E. L. Dieperink, O. Scholten, and F. Iachello, Phys. Rev. Lett. **44**, 1747 (1980).
[26] H. J. Lipkin, N. Meshkov, and A. J. Glick, Nucl. Phys. **62**, 188 (1965).
[27] O. S. van Roosmalen, R. D. Levine, and A. E. L. Dieperink,

Chem. Phys. Lett. **101**, 512 (1983).
[28] O. S. van Roosmalen, Ph.D. thesis, University of Groningen, 1982.
[29] M. A. Caprio, J. Phys. A **38**, 6385 (2005).
[30] H. E. Stanley, *Introduction to Phase Transitions and Critical Phenomena* (Oxford Science, New York, 1971).
[31] F. Iachello and N. V. Zamfir, Phys. Rev. Lett. **92**, 212501 (2004).
[32] M. A. Caprio, P. Cejnar, and F. Iachello, Ann Phys. (to be published).
[33] *Finite Size Scaling*, edited by J. L. Cardy (North-Holland, Amsterdam, 1988).
[34] M. E. Fisher, in *Proceedings of the International School of Physics "Enrico Fermi,"* edited by M. S. Green (Academic, New York, 1972), Course LI.
[35] M. E. Fisher and M. N. Barber, Phys. Rev. Lett. **28**, 1516 (1972).
[36] F. Iachello, in *From Nuclei and Their Constituents to Stars: Proceedings of the International School of Physics "Enrico Fermi*," edited by A. Molinari, L. Riccati, W. M. Alberico, and M. Morando (IOS, Amsterdam, 2003), Course CLIII.
[37] F. Iachello, Phys. Rev. Lett. **85**, 3580 (2000).
[38] F. Iachello, Phys. Rev. Lett. **87**, 052502 (2001).
[39] R. F. Casten and N. V. Zamfir, Phys. Rev. Lett. **85**, 3584 (2000).
[40] R. F. Casten and N. V. Zamfir, Phys. Rev. Lett. **87**, 052503 (2001).
[41] D. J. Rowe, P. S. Turner, and G. Rosensteel, Phys. Rev. Lett. **93**, 232502 (2004).
[42] S. Dusuel, J. Vidal, J. M. Arias, J. Dukelsky, and J. E. García-Ramos, Phys. Rev. C **72**, 011301(R) (2005).
[43] J. M. Arias, J. Dukelsky, J. E. García-Ramos, and J. Vidal, Phys. Rev. C **75**, 014301 (2007).
[44] R. S. Berry, C. R. Phys. **3**, 319 (2002).
[45] M. Winnewisser, B. P. Winnewisser, I. R. Medvedev, F. C. D. Lucia, S. C. Ross, and L. M. Bates, J. Mol. Struct. **798**, 1 (2006).
[46] F. Pérez-Bernal and F. Iachello (unpublished).
[47] L. M. Bates, ZAMP **42**, 837 (1991).
[48] D. A. Sadovskii and B. Zhilinskii, Phys. Lett. A **256**, 235 (1999).
[49] R. Cushman and D. A. Sadovskii, Physica D **142**, 166 (2000).
[50] P. Cejnar, M. Macek, S. Heinze, J. Jolie, and J. Dobes, J. Phys. A **39**, L515 (2006).
[51] S. Heinze, P. Cejnar, J. Jolie, and M. Macek, Phys. Rev. C **73**, 014306 (2006).
[52] M. Macek, P. Cejnar, J. Jolie, and S. Heinze, Phys. Rev. C **73**, 014307 (2006).
[53] M. S. Child, T. Weston, and J. Tennyson, Mol. Phys. **96**, 371 (1999).
[54] G. Herzberg, *Molecular Spectra and Molecular Structure, Vol. II: Infrared and Raman Spectra of Polyatomic Molecules* (Van Nostrand-Reinhold, New York, 1945).
[55] D. Kusnezov, J. Chem. Phys. **101**, 2289 (1994).
[56] M. Angelova, Phys. Part. Nucl. **33**, S37 (2002).
[57] M. Angelova and A. Frank, Phys. At. Nucl. **68**, 1625 (2005).
[58] A. Arima and F. Iachello, Ann. Phys. **123**, 468 (1979).
[59] E. Santopinto, R. Bijker, and F. Iachello, J. Math. Phys. **37**, 2674 (1996).
[60] M. Abramowitz and I. A. Stegun, *Handbook of Mathematical Functions* (Dover, New York, 1965).